PHYSICAL REVIEW D **80,** 044007 (2009)

Group field theory renormalization in the 3D case: Power counting of divergences

Laurent Freidel* and Razvan Gurau†
Perimeter Institute for Theoretical Physics, 31 Caroline St, Waterloo, Ontario N2L 2Y5, Canada

Daniele Oriti‡
Perimeter Institute for Theoretical Physics, 31 Caroline St, Waterloo, Ontario N2L 2Y5, Canada
and Albert Einstein Institute, Am Muehlenberg 4, Golm, Germany, EU
(Received 1 June 2009; published 11 August 2009)

We take the first steps in a systematic study of group field theory (GFT) renormalization, focusing on the Boulatov model for 3D quantum gravity. We define an algorithm for constructing the 2D triangulations that characterize the boundary of the 3D bubbles, where divergences are located, of an arbitrary 3D GFT Feynman diagram. We then identify a special class of graphs for which a complete contraction procedure is possible, and prove, for these, a complete power counting. These results represent important progress towards understanding the origin of the continuum and manifoldlike appearance of quantum spacetime at low energies, and of its topology, in a GFT framework.

DOI: 10.1103/PhysRevD.80.044007 PACS numbers: 04.60.−m, 04.60.Pp

I. INTRODUCTION

The field of nonperturbative quantum gravity is progressing fast, in several directions [1]. Spin foam models [2] are one of them, and can be understood as a covariant formulation of the dynamics of loop quantum gravity [3] and as a new algebraic implementation of discrete quantum gravity approaches, such as Regge calculus [4] and dynamical triangulations [5]. The basic idea is to encode quantum gravity kinematics in discrete quantum histories given by *spin foams*: combinatorial two complexes labeled by group-theoretic data. The two complex is combinatorially dual to a simplicial complex, of which the algebraic data determine a possible geometry. A quantum dynamics is specified by the assignment of a probability amplitude to each spin foam, and the model is defined by a sum over both two complexes and corresponding algebraic data. At present the most complete definition of a spin foam model is achieved by means of the so-called group field theory formalism [6–8].

Group field theories are quantum field theories over group manifolds, characterized by a nonlocal pairing of field arguments in the action, which can be seen as a generalization of matrix models [9] (and of the subsequent, but less developed, tensor models [10–12]). The combinatorics of the field arguments in the interaction term of the group field theory (GFT) action follows that of $(D-2)$ faces of a D simplex, with the GFT field itself interpreted as a (second) quantization of a $(D-1)$ simplex. The kinetic term of the action governs the gluing of two D simplices along a common $(D-1)$ simplex; see [7,8] for details. Because of this combinatorial structure, the GFT Feynman diagrams, themselves cellular complexes, are dual to D-dimensional simplicial complexes, as we will discuss at length in the following. Thus GFTs can be seen [6,7] as a simplicial ''third quantization'' of gravity [13], in which a discrete spacetime emerges as a Feynman diagram of the theory in perturbative expansion. The field arguments assign group-theoretic data to these cellular complexes, and the GFT perturbative expansion in Feynman amplitudes defines uniquely and completely [14] a spin foam model. This makes GFTs a very useful tool, but also suggests that they may provide a more fundamental definition of a dynamical theory of spin networks, representing the best way to investigate nonperturbative and collective properties of their quantum dynamics [6,7,15]. The results we present in this paper are a first step in realizing this suggestion, in the simpler 3D context.

The main open problem that GFTs, as well as other discrete quantum gravity approaches, face is that of bridging the gap between their discrete description of spacetime and the one we are accustomed to at low energy, based on continuum manifolds whose geometry is governed by a classical field theory like general relativity. As it is immediately clear, several issues are intertwined here. First of all, there is the issue of obtaining a *continuum* description of spacetime from the discrete structures that GFTs generate in its stead, i.e., the GFT Feynman diagrams. This means understanding in which regime of the fundamental GFT model a continuum approximation is allowed and useful to study spacetime physics. Two more technical issues are related to the fact that GFTs define a sum over simplicial complexes, representing, as we said, discrete spacetime structures, (1) of arbitrary topology and (2) not necessarily corresponding to manifolds [16]. In general, in fact, they fail to satisfy manifold conditions and correspond to pseudomanifolds instead, i.e., contain conical singularities at the vertices. So one can ask why at low energy and in the continuum approximation does space-

*lfreidel@perimterinsitute.ca
†rgurau@perimeterinstitute.ca
‡daniele.oriti@aei.mpg.de

time have a fixed (and trivial) topology and manifold properties? Both questions can and should be addressed in the GFT formalism. The first has an analogue in the context of matrix models, where it is known that diagrams of trivial topology (S^2 in the compact case) dominates the Feynman amplitudes of the theory in the so-called double-scaling limit [9]. The second arises only in dimensions $D > 2$ [16] and is known not to be easily solvable in the context of tensor models (the immediate generalization of matrix models) [10,11], which are characterized by trivial Feynman amplitudes, i.e., amplitudes which depend only on the combinatorics of the underlying simplicial complex. We touch on the second of these two issues, and provide some clues towards its solution, in this paper. Obviously, all of these open issues are dynamical in nature, i.e., depend heavily on the quantum amplitudes of the specific GFT model one considers. This is even more true for the most important of the open problems of this approach: to reproduce a continuum manifold of some topology representing spacetime is not enough, as we want the dynamics of its geometry to be governed by general relativity (possibly up to quantum corrections to the same). We do not touch on this last issue in this paper, and we refer to the literature for discussions, ideas and partial results concerning it [3,6,15].

GFTs offer a very convenient framework for investigating all of the above issues, common to many different quantum gravity approaches, for a variety of reasons. An important one is that GFTs are almost ordinary quantum field theories, their only (if crucial) peculiarity being a complicated (nonlocal) combinatorial structure of arguments in the action and the corresponding simplicial nature of associated Feynman diagrams. Still, they allow the application of standard and very powerful quantum field theory ideas and methods to tackle quantum gravity problems, like the ones mentioned above. These methods will have to be suitably generalized to the new context, of course, and the consequences of their application reinterpreted in quantum gravity terms.

Among the quantum field theory methods that seem most suited to tackle these more technical issues, as well as to study the general problem of the (collective) dynamics of GFT models in different regimes, is the renormalization group. In this paper we start a systematic study of GFT renormalization, focusing on a simple and well-known model, the Boulatov model for 3D quantum gravity [17]. It will allow us to develop some tools that can be later applied to other models, and to obtain a first understanding of some of the difficulties involved in applying renormalization ideas to GFTs. We will see, in fact, that this model is highly nontrivial already, and that the complicated combinatorial and topological structure of its Feynman diagrams makes each step of the usual renormalization procedures much less straightforward, but also more interesting, than in usual quantum field theories. More precisely, the divergences of this model are related to the topology of the bubbles (three-dimensional cells) in the Feynman diagrams, and a general power counting theorem is very difficult to establish mainly due to the very complicated topological structure of 3D simplicial complexes.

Focusing on the Boulatov model allows us also to make the first steps in understanding the role of topological invariance in GFT and in quantum gravity in general, from the point of view of renormalization. In the GFT context, that fact that the Boulatov model corresponds to a quantization of BF theory, a topological quantum field theory, translates into the property that its Feynman amplitudes depend only on the topology of the corresponding Feynman diagram, but not on its specific combinatorial structure for given topology. From the spin foam point of view, this is the well-known triangulation independence property of the Ponzano-Regge model. We expect the renormalization group to provide a new field-theoretic interpretation of this feature. More precisely, we conjecture the following scenario: topological invariance should give rise to a nontrivial fixed point of the renormalization group, and with the property that the model is dominated, in its vicinity, by simple manifold configurations. In fact, usually fixed points correspond to new symmetries, e.g., the Langmann-Szabo symmetry in nonidentically distributed matrix models [18]; also, looking again at matrix models [9], one sees that the renormalization group identifies the most regular diagrams, planar diagrams, as the dominant ones; we look for a similar feature in the more general GFT setting, as we discuss in the following. We actually expect more: that also in higher dimensions, and for GFT models that are not themselves topological, i.e., for quantum gravity model obtained, for example, by constraining appropriately topological BF models, like most current spin foam/GFT models [19–22], one will find nontrivial fixed points corresponding to a topological phase.

A systematic development of GFT renormalization requires defining first of all the GFT counterpart of the basic ingredients of the renormalization of quantum field theories. These are: (a) a scale analysis; (b) a locality principle; (c) a power counting of divergences. A partial power counting of divergences for the Boulatov model is our main result, and it is obtained by addressing the issues of scale and of locality first.

As far as scales are concerned, we use the spectral decomposition of the GFT propagator (a simple product of delta functions in this model) in order to introduce them easily, by an explicit cutoff. This induces a departure from topological invariance, i.e., it does not respect exactly the initial symmetries of the model, but allows one to identify nicely the divergent contributions to the amplitudes (a similar cutoff procedure, which however maintains topological invariance, would be to use quantum groups and work with the Turaev-Viro model [17,23]).

A locality principle, in the context of renormalization, is needed only for the divergent graphs: the amplitude of such

graphs must be combined with local counterterms in order to become finite. It is crucial for our purposes to note that in all known models, the local nature of the field theories translates into the existence of a contraction procedure for the Feynman diagrams. In usual quantum field theories, all connected graphs can be contracted to points exactly because of locality, and hence can be combined with counterterms. Similarly both in matrix models [9], and noncommutative quantum field theory models [24] the only divergences in the amplitudes come from planar graphs, and these are also the class of graphs that can be contracted, thus are in some sense local, so that once more they can be combined with counterterms and renormalized. This suggests that the point of view on locality, diagram contraction, and renormalization can be reversed. Take for instance an arbitrary matrix model, not necessarily identically distributed. Even before establishing a power counting theorem, the following question is legitimate: is there a family of graphs which can be fully contracted? The answers is that planar graphs are the only ones for which a complete and consistent contraction procedure can be defined. Hence, if a matrix model is to allow for the application of renormalization group procedure and thus be renormalized in the standard sense, all its divergent, and thus the only relevant, graphs must be planar. However, we know very well by now that, in order to reach the point where renormalization can be applied, i.e., in order to be in the regime in which only planar graphs are relevant, for a given matrix model, one might need further ingredients. For instance, for a model of identically distributed matrices one must introduce a scaling limit [9]. We apply this reasoning to the 3D Boulatov GFT model, and ask: is there a family of graphs on which one could define a full contraction procedure? In light of our proof of power counting we can give a definite answer. We show that the only family of graph for which a full contraction procedure exists are the ''type 1'' manifolds defined in Sec. III. Hence, in order to be able to define a renormalization group for this model, all divergent diagrams should be type 1. The need for a contraction procedure in the context of GFT renormalization also explains why we do not try to define a simpler, global proof for the degree of divergence of GFT diagrams, and look instead for one based on this contraction, even if, as we will see, it turns out to be rather involved.

Anyway, as anticipated, for these type 1 diagrams, we are able to define this complete contraction procedure and prove a corresponding power counting theorem for their divergences. As a first step in the process of defining the contraction and identifying divergences, we will give an algorithm for constructing the 2D triangulations that characterize the boundary of the 3D bubbles of an arbitrary 3D GFT diagram graph. We believe that this algorithm is an interesting and useful result in itself. As mentioned, it is in fact at these bubbles that the divergences of the model are located. However, as we will see, and as it is the case with matrix models, the power counting we establish is not uniform in the number of internal vertices. We then conjecture that in order to define a renormalization group for GFT models we again need to take an appropriate scaling limit. We also note that this result cannot be extended to arbitrary manifold configuration (as it will be shown on a counterexample).

II. THE BOULATOV MODEL REVISED

We start defining the model, i.e., the group field theory defined by Boulatov [17] for 3D Riemannian quantum gravity. Like in any other group field theory, each field, here a function $\phi(g_1, g_2, g_3)$: $SU(2)^{\times 3} \rightarrow \mathbb{R}$, is interpreted as representing a $(D-1)$ simplex, here a triangle, and the crucial feature of the action is that the combinatorics of field arguments in the kinetic and interaction term is chosen in such a way that the Feynman diagrams of the theory are cellular complexes that are topologically dual to simplicial complexes, three-dimensional ones in this specific case. The Feynman amplitudes of this field theory, i.e., the corresponding spin foam model, are products of delta functions, each of them associated to a face of the Feynman diagram representing a discrete spacetime. The arguments of these a delta functions are the holonomies of an $SU(2)$ connection associated to the face. The model reproduces, in its perturbative expansion, the (trivial) geometric content of 3D gravity discretized on the simplicial complex dual to each Feynman diagram (flatness of the gravitational connection). The corresponding spin foam formulation is the well-known Ponzano-Regge model [25].

In order to simplify our analysis we will look at an ''orientable'' version of the Boulatov model (meaning that the simplicial complexes dual to its graphs are orientable).

We consider a tetrahedron labeled as in Fig. 1(a), and we orient all triangles consistently with the exterior normals of the tetrahedron. Thus the four oriented triangles are (1, 2, 3), (3, 4, 5), (5, 6, 1), and (6, 4, 2), and these become the labeling of arguments of the four fields in the interaction

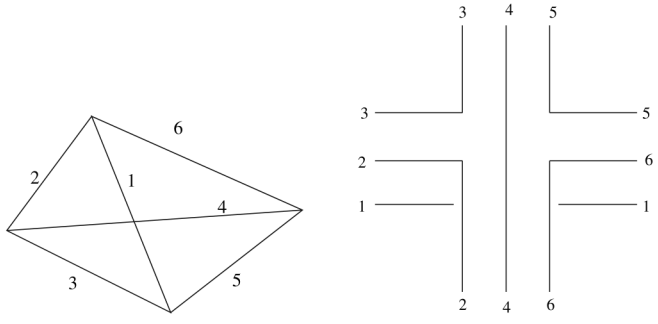

(a) Labeled tetrahedron. (b) Labeled four valent vertex.

FIG. 1. The GFT vertex.

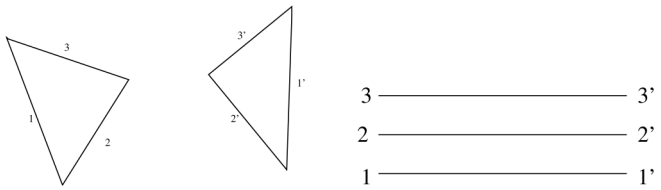

(a) Labeled triangles. (b) Labeled propagator.

FIG. 2. The GFT propagator.

term of the action. Notice that taking into account the orientation of the tetrahedra results in a specific pairing of the group variables (field arguments) in the interaction term. Moreover this pairing is *different* from the naive pairing which is usually prescribed. As said, our choice is dictated by the fact that we want all normals associated to the triangles of the tetrahedron oriented outwards. The dual of the tetrahedron is the four-valent vertex of the GFT action. Labeling the vertex clockwise we end up with the picture drawn in Fig. 1(b). The lines in the vertex (1, 2,. . ., 6) will henceforth be referred to as strands.

Two tetrahedra are glued along triangles. The identification of the two triangles (1, 2, 3) and $(3', 2', 1')$ in Fig. 2(a) gives $1 = 1'$, $2 = 2'$, and $3 = 3'$. This identification is reproduced by the GFT propagator, represented in 2(b).

Thus the GFT whose graphs are orientable in the sense above is given by the action

$$S = \frac{1}{2}\int dg_1 dg_2 dg_3 \phi(g_1, g_2, g_3)\phi(g_3, g_2, g_1) + \frac{\lambda}{4}\int \phi(g_1, g_2, g_3)\phi(g_3, g_4, g_5)\phi(g_5, g_6, g_1) \times \phi(g_6, g_4, g_2), \quad (1)$$

where the field ϕ, that we take as real valued, is *not* assumed to have specific symmetry properties under permutations of its three arguments; that is, unlike [16,26] we associate to each line in a Feynman diagram only the identity permutation. The integrations over the group (left implicit in the interaction term) are performed with the invariant Haar measure.

The propagator of our model is thus

$$P(g_1, g_2, g_3; g_{3'}, g_{2'}, g_{1'}) = \int dh \delta(g_1 h g_{1'}^{-1})\delta(g_2 h g_{2'}^{-1}) \times \delta(g_3 h g_{3'}^{-1}), \quad (2)$$

imposing the simple identification of arguments we mentioned.

The model is then defined, at the quantum level, by the partition function, expanded in perturbation theory as

$$Z = \int \mathcal{D}\phi e^{-S[\phi]} = \sum_{\mathcal{G}} \frac{\lambda^N}{\mathrm{sym}[\mathcal{G}]} A(\mathcal{G}),$$

where N is the number of interaction vertices in the Feynman graph $\mathcal{G}$, $\mathrm{sym}[\mathcal{G}]$ is a symmetry factor for the graph, and $A(\mathcal{G})$ the corresponding Feynman amplitude.

Having identified the propagator and vertex function of the model, we can now construct the Feynman amplitudes. However, these being given by products of delta functions on the $SU(2)$ group, some regularization is needed in order to have them well defined. There exists several regularizations of the Boulatov model. The best known is the Turaev-Viro model, obtained by switching from $SU(2)$ to its quantum deformation $SU(2)_q$ with q a root of unity [17,23]; this model is known to be related to 3D Riemannian quantum gravity with positive cosmological constant; the quantum deformation has the immediate effect of restricting the representation summed over in the mode expansion of the Feynman amplitudes to a finite range, thus imposing an infrared regulator (associated to the cosmological constant). Another possible regularization is obtained by substituting each delta function in the propagator with a heat kernel on the group, with (temperature) parameter β; this corresponds to leaving the range of representations summed over in momentum space unrestricted, but inserting in it a regularizing factor $e^{(1/\beta)j(j+1)}$; for $\beta \to \infty$ one recovers the original model. Looking instead directly at the Feynman (spin foam) amplitudes of the model, one can use another regularization that involves inserting appropriate factors associated to vertices to the simplicial complex dual to the Feynman diagram [25,27–29]. These factors can be interpreted [27,28] as the volume of the gauge group associated to the translation symmetry of discretized BF, and this regularization becomes then a gauge fixing procedure for this symmetry. It is not clear, however, how to implement this last regularization procedure at the GFT level, ultimately because we do not know yet how to identify the translation symmetry at the level of the Boulatov action. Here we choose a different one. Let Λ be a large number, we define the cutoffed propagator like

$$P^{\Lambda}(g_1, g_2, g_3; g_{3'}, g_{2'}, g_{1'}) = \int dh \delta^{\Lambda}(g_1 h g_{1'}^{-1}) \times \delta^{\Lambda}(g_2 h g_{2'}^{-1})\delta^{\Lambda}(g_3 h g_{3'}^{-1}), \quad (3)$$

with

$$\delta^{\Lambda}(h) = \sum_{j=0}^{\Lambda} d_j \chi^j(g). \quad (4)$$

The nice feature of this regularization is that, on top of being very simple, it preserves the composition properties of the delta functions (as the heat kernel regularization does), and also allows easy evaluations of amplitudes

(which are instead a bit more complicated with the heat kernel regularization). Using the explicit form of our regularized δ functions we can prove, for example, the following two properties:[1]

$$\int dh \delta^{\Lambda}(gh^{-1})\delta^{\Lambda}(hg'^{-1}) = \delta^{\Lambda}(gg'^{-1}), \tag{5}$$

$$\int dh \delta^{\Lambda}(gh) = 1. \tag{6}$$

A graph $\mathcal{G}$ of this model is formed of the vertices and propagators drawn in 1(b) and 2(b). We denote $V_{\mathcal{G}}$ the set of internal vertices (labeled $V_1, \ldots V_{|V_{\mathcal{G}}|}$), $L_{\mathcal{G}}$ the set of internal lines (labeled $L_1, \ldots L_{|L_{\mathcal{G}}|}$). The closed circuits in the graph correspond to faces. We denote $F_{\mathcal{G}}$ the set of internal faces (labeled $F_1, \ldots F_{|\mathcal{F}_{\mathcal{G}}|}$). Finally, closed three-dimensional regions of the graph are called bubbles. We denote $B_{\mathcal{G}}$ the set of internal bubbles (labeled $B_1, \ldots B_{|B_{\mathcal{G}}|}$).

In order to write the amplitude of a graph we chose an orientation for each of its lines and faces. The amplitude of a graph then writes (in self-explaining notations) as

$$\lambda^{|V_{\mathcal{G}}|} A(\mathcal{G}) = \lambda^{|V_{\mathcal{G}}|} \Big(\int \prod_{L \in L_{\mathcal{G}}} dh_L \prod_{F \in F_{\mathcal{G}}} \delta^{\Lambda} \Big(\overleftarrow{\prod_{L \in \partial F}} h_L \Big) \Big) \tag{7}$$

with h_L or h_L^{-1} chosen in the argument of the δ function corresponding to the face F according to whether the orientation of F coincides or not with that of the line L. The arrow over the product expresses that the product is an order product over the lines in ∂F in the order that is induced by the orientation of F.

III. BUBBLES

A. Labeling the bubbles

Each Feynman diagram will be given by construction, as we said, by a cellular complex dual to a three-dimensional simplicial complex. The vertices, lines, and faces of this graph $\mathcal{G}$, dual, respectively, to tetrahedra, triangles, and edges of the simplicial complex, are readily identified. On the contrary the three cells, also called ''bubbles'' and dual to the vertices of the simplicial complex, are difficult to identify. In this section we present the algorithm which allows one to identify them, first of all, and construct a graph which characterizes the combinatorial structure of each bubble of a generic graph $\mathcal{G}$. This will be crucial for our contraction procedure, and for establishing our power counting theorem. It also allows one to determine easily the topology of the boundary of each bubble of $\mathcal{G}$, and let us stress that identifying this boundary topology is the ingredient needed to determine whether the simplicial complex dual to each graph $\mathcal{G}$ is a simplicial manifold or not. Indeed, the necessary and sufficient condition for such a simplicial complex to be a manifold is that every one of its bubbles has the topology of a three ball, i.e., that their boundaries are two-spheres.

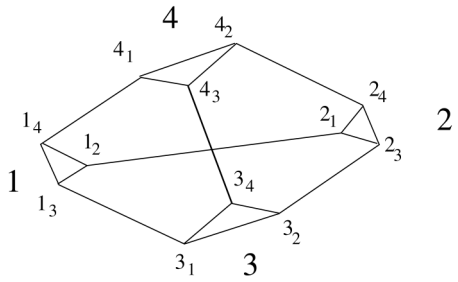

FIG. 3. Fully labeled truncated tetrahedron.

The basic idea is the following. Since bubbles of $\mathcal{G}$ are dual to the vertices of its dual simplicial complex, we can define a triangulation of their boundary in such a way that each tetrahedron in the simplicial complex corresponds to a triangle. The way to visualize it is that we carve out a small spherical neighborhood of each vertex of the initial triangulation. This corresponds to carving out each corner of the tetrahedra like in Fig. 3. Gluing back these truncated tetrahedra we obtained a 3D triangulation with a 2D boundary which is also triangulated.

The topological elements of the tetrahedron, and of the simplicial complex it belongs to, are referred to as ''three dimensional.'' They are labeled as follows (see Fig. 3)

(i) The vertices of the tetrahedron (3D vertices) are labeled by numbers 1, 2, 3, and 4.
(ii) The edges of the tetrahedron (3D edges) connect two vertices, hence will be denoted by unordered couples of numbers.[2] For instance, the line connecting vertices 1 and 2 is denoted (1,2), etc …
(iii) The triangles of the tetrahedron (3D triangles) are formed by three vertices and three edges. We denote them by ordered triples of numbers (associated to vertices) (3, 4, 1), (3, 1, 2), (3, 2, 4), and (4, 2, 1). Each triangle has a boundary identified by a set of edges. For instance, the edges in the boundary of the triangle (3, 4, 1) are (3, 4), (4, 1), and (1, 3).
(iv) The tetrahedron itself (3D tetrahedron) is denoted (1, 2, 3, 4), i.e., it is identified by the unordered set of its four vertices.

In order to identify the bubbles we must then deal with two distinct simplicial complexes. In fact, besides the 3D simplicial complex of tetrahedra glued along their boundary triangles, we need to consider also a second simplicial complex, made of the small triangles carved in Fig. 3 glued along their boundary edges. We now explain a convenient labeling of the elements of this second simplicial complex and their relation with the original 3D one. The topological

[1]The properties follow from $\int dh D^{j'}_{m'n'}(h)\bar{D}^{j}_{mn}(h) = \frac{1}{d_j}\delta^{jj'}\delta_{m'm}\delta_{n'n}$.

[2]The edge orientation is irrelevant because each 3D edge is assigned a different orientation in the two triangle it belongs to.

elements of the small triangles are called ''two dimensional'' (2D) and are labeled as follows (see Fig. 3):

(i) The vertices of the small triangles (2D vertices) are labeled by a number and an index. The number keeps track of the 3D vertex of the tetrahedron to which the small triangle is associated, while the index indicates the 3D edge of the tetrahedron transverse to the 2D vertex. Thus the 2D vertex 1_2 belongs to the triangle corresponding to the 3D vertex 1, and transverse to the 3D edge (1, 2), while the 2D vertex 1_3 belongs to the triangle associated with the 3D vertex 1 and is touched by the 3D edge (1, 3).

(ii) The edges of the small triangles (2D lines) are labeled by a couple of 2D vertices. Thus $(1_2, 1_3)$ is the edge going from 1_2 to 1_3.

(iii) The small triangles (2D triangles) are labeled by their vertices $(1_2, 1_3, 1_4)$, $(2_1, 2_4, 2_3)$, $(3_1, 3_2, 3_4)$, and $(4_1, 4_3, 4_2)$; these 2D triangles are oriented, again with outward normals.

All the topological elements of the 2D complex (connected components, vertices, edges, triangles) are obtained by ''projecting'' those of the 3D simplicial complex (vertices, edges, triangles, tetrahedra)

Consider the projection of the elements of a single tetrahedron. From Fig. 3 we see that

(i) The oriented 3D tetrahedron (1, 2, 3, 4) projects into *four* oriented 2D triangles $(1_2, 1_3, 1_4)$, $(2_1, 2_4, 2_3)$, $(3_1, 3_2, 3_4)$, and $(4_1, 4_3, 4_2)$.

(ii) Each 3D triangles [i.e., (3, 4, 1), (3, 1, 2), (3, 2, 4), or (4, 2, 1) which are faces of the 3D tetrahedron] project into *three* oriented 2D edges. Thus the triangle (3, 4, 1) projects into the lines $(3_4, 3_1)$, $(4_1, 4_3)$, and $(1_3, 1_4)$, while (3, 1, 2) projects into $(3_1, 3_2)$, $(1_2, 1_3)$, and $(2_3, 2_1)$, and so on.

(iii) Each one of the six 3D edges of the tetrahedron (1, 2), (1, 3), (1, 4), (2, 3), (2, 4), and (3, 4) project each into *two* 2D vertices. (1, 2) projects into the vertices 1_2 and 2_1, (1, 3) projects into the vertices 1_3 and 3_1, and so on.

(iv) Each vertex of the 3D tetrahedron 1, 2, 3, and 4 projects to *one* 2D connected component (a 2D triangle).

The 3D topological elements are called ''ancestors'' of those obtained by projection to the 2D simplicial complex (and the latter are the descendents of the former). A 3D tetrahedron has for instance four 2D triangle descendents, a 3D triangle has three 2D edges descendents, and so on.

The two simplicial complexes are dual to graphs. The 3D complex is dual to a 3D GFT graph $\mathcal{G}$, while the 2D simplicial complex is dual to the 2D graph, called $\bar{\mathcal{G}}$. A 3D GFT graph $\mathcal{G}$ is a fat graph carrying three strands per edge while a 2D graph is a fat graph carrying two strands per edge.

The dual of a tetrahedron is the GFT vertex. In the triangulation representation each 3D edge projects into two vertices in the 2D complex. The 3D edges of the tetrahedron are dual to faces made up of 3D strands, while the 2D vertices are dual to faces made up of 2D strands. Consequently in the graph picture, each 3D strand in the 3D dual vertex projects into two 2D strands, one on the left and one on the right. The fully labeled dual of the tetrahedron from Fig. 3 is drawn in Fig. 4, with the 2D strands represented by dashed lines.

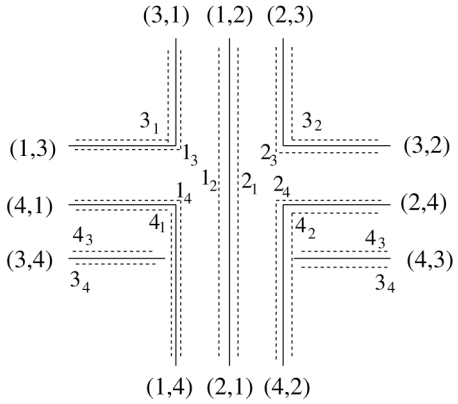

FIG. 4. Fully labeled 3D interaction (dual vertex).

We can now translate trivially the projection at the level of 3D and 2D graphs.

(i) The 3D dual vertex (1, 2, 3, 4) projects into *four* 2D dual vertices $(1_2, 1_3, 1_4)$, $(2_1, 2_4, 2_3)$, $(3_1, 3_2, 3_4)$, and $(4_1, 4_3, 4_2)$.

(ii) Each one of the four 3D dual half-lines (3, 4, 1), (3, 1, 2), (3, 2, 4), and (4, 2, 1) projects into *three* 2D dual half-lines. (3, 4, 1) projects into the $(3_4, 3_1)$, $(4_1, 4_3)$, and $(1_3, 1_4)$, etc.

(iii) Each one of the 3D strands (3, 4), (4, 1), (1, 3), (1, 2), (2, 3), and (2, 4) projects into *two* 2D strands. (3, 4) projects into 3_4 and 4_3, (4, 1) projects into 4_1 and 1_4, etc.

(iv) Each 3D bubble projects into *one* 2D connected component (connected surface whose dual is made out of 2D triangles); this 2D connected component, as we have noted above, characterizes the topology of the boundary of the bubble, and thus allows one to determine if the 3D simplicial complex satisfies manifold conditions or not.

The 3D graph $\mathcal{G}$ is formed of 3D vertices and 3D lines. The 3D lines are identifications of two 3D half-lines. The 2D descendents of a 3D line are then obtained by identifying the 2D descendents of the two 3D half-lines.

The algorithm to draw the 2D projection $\bar{\mathcal{G}}$ of a 3D graph $\mathcal{G}$ is then the following. Start by drawing the 2D descendents of all 3D dual vertices. Each 3D dual vertex will give four such descendents (see Fig. 5). Draw all descendents of the 3D dual lines. Each 3D dual line will have three descendents (see Fig. 6). Connect the 2D dual vertices using the 2D dual lines. The 3D dual faces of the graph

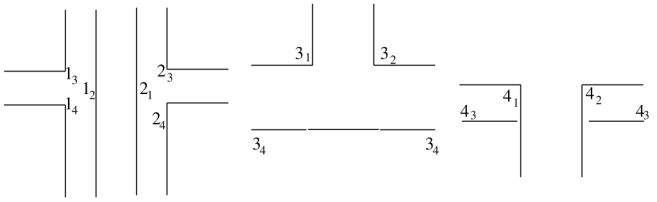

FIG. 5. 2D dual vertices descendent from a 3D dual vertex.

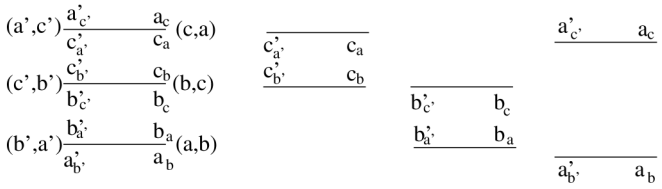

FIG. 6. 2D dual lines descending from a 3D dual line.

$\mathcal{G}$ are closed 3D strands while the 2D dual faces of $\bar{\mathcal{G}}$ are closed 2D strands.

We conclude this section by presenting in detail an example of a 3D graph and its 2D projection. Consider the ''sunshine'' graph, denoted $\mathcal{G}_1$, drawn in Fig. 7.

To simplify the figures we drop the indices of the labels and denote the strands of the 2D projection of the vertex on the left, call it V, 1 to 12 and those of the vertex on the right, call it V', $1'$ to $12'$. We start by identifying the 2D descendents of the two 3D vertices. The descendents of V are (1, 2, 3), (4, 5, 6), (7, 8, 9), and (10, 11, 12), whereas the descendents of V' are $(1', 2', 3')$, $(4', 5', 6')$, $(7', 8', 9')$, and $(10', 11', 12')$.

We now consider one descendent of V, say (4, 5, 6). Its half-line (45) is connected to the half-line $(3', 2')$ of the 2D descendent $(1', 2', 3')$ of V' by a 2D descendent of the line L_3. Therefore the two vertices (4, 5, 6) and $(1', 2', 3')$ fall in the same bubble (2D connected component). We continue by analyzing the remaining half-lines of the two vertices. The half-line (5, 6) is connected to $(2', 1')$ by a descendent of the line L_2 and (6, 4) is connected to $(1', 3')$ by a descendent of the line L_1. As these 2D vertices and lines

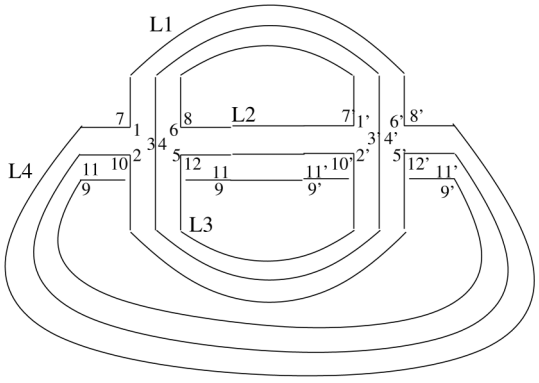

FIG. 7. The sunshine graph $\mathcal{G}_1$.

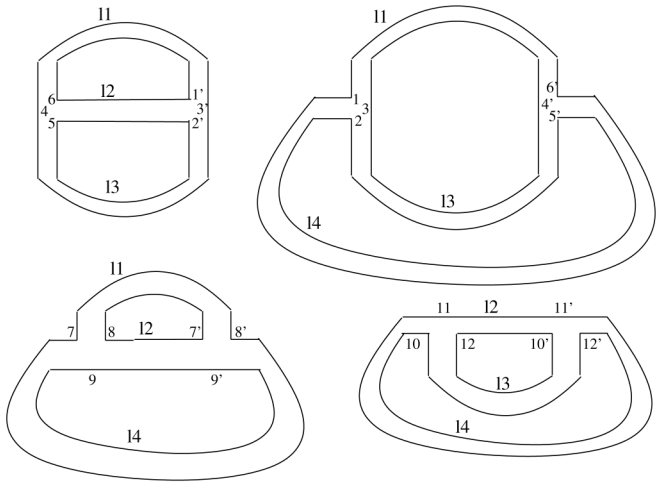

FIG. 8. The 2D projection $\bar{\mathcal{G}}_1$.

form a closed connected component they represent a bubble, which we draw in the upper left corner of Fig. 8. The other bubbles are obtained in a strictly parallel manner.

B. Characterizing the bubbles

From now on, we stop labeling elements of $\mathcal{G}$ and $\bar{\mathcal{G}}$ as ''dual'' for simplicity. This can be done without confusion because, from now on, we refer only on the 3D and 2D graphs $\mathcal{G}$ and $\bar{\mathcal{G}}$, leaving aside their corresponding simplicial complexes.

Let $V_{\mathcal{G}}$, $L_{\mathcal{G}}$, $F_{\mathcal{G}}$, $B_{\mathcal{G}}$ label the sets of vertices, lines, faces, and bubbles of the 3D GFT graph $\mathcal{G}$. Similarly we denote by $v_{\mathcal{G}}$, $l_{\mathcal{G}}$, $f_{\mathcal{G}}$, $b_{\mathcal{G}}$ the sets of vertices, lines, faces, and connected components, of the 2D graph $\bar{\mathcal{G}}$ obtained by the projection procedure. We then have the relations

$$\begin{aligned} |v_{\mathcal{G}}| &= 4|V_{\mathcal{G}}| \qquad |l_{\mathcal{G}}| = 3|L_{\mathcal{G}}| \\ |f_{\mathcal{G}}| &= 2|F_{\mathcal{G}}| \qquad |b_{\mathcal{G}}| = |B_{\mathcal{G}}|. \end{aligned} \tag{8}$$

A first consequence of the above equalities is the following. For any 2D graph $\bar{\mathcal{G}}$ we can express the Euler characteristic of the 2D surface it represents in terms of an alternating sum of elements:

$$|v_{\mathcal{G}}| - |l_{\mathcal{G}}| + |f_{\mathcal{G}}| = 2|b_{\mathcal{G}}| - 2\sum_{b\in b_{\mathcal{G}}} g_b, \tag{9}$$

with g_b the genus of the connected component b (which is the boundary of some given bubble of the 3D graph $\mathcal{G}$).

Suppose that the 3D graph $\mathcal{G}$ is a vacuum graph. Since the 3D GFT graph is four valent we have $2|V_{\mathcal{G}}| = |L_{\mathcal{G}}|$. Substituting Eq. (8) into Eq. (9) and using this relation yields the identity

$$|V_{\mathcal{G}}| - |L_{\mathcal{G}}| + |F_{\mathcal{G}}| - |B_{\mathcal{G}}| = -\sum_{B\in B_{\mathcal{G}}} g_B, \tag{10}$$

with g_B the genus of the boundary of the bubble B. The left-hand side of this identity is the Euler characteristic of

the simplicial complex dual to the 3D GFT graph. It is zero if and only if this simplicial complex is a simplicial manifold. Equivalently this means that a 3D closed graph represents a manifold if all the bubbles are spherical ($g_B = 0$). This is a well-known condition that insures that the neighborhood of each vertex of the triangulation is isomorphic to a three ball. If one of the bubble duals to a vertex is *not* spherical the neighborhood of this vertex contains a noncontractible torus or genus g surface and the corresponding simplicial complex is only a pseudomanifold.

The purpose of this work is to understand better the renormalization properties of the amplitude (7). As can been seen from its definition, the divergences are related to the presence of the delta function for each face, while naively each integration can potentially kill one delta function. A closer look shows that because the integrand is invariant under gauge transformations acting at the vertices of the graph not all the integrations over g_L can kill the delta functions, only at most $|L_{\mathcal{G}}| - |V_{\mathcal{G}}| + 1$. Thus it looks that the behavior of the integral is characterized by a naive degree of divergence given by $|F_{\mathcal{G}}| - |L_{\mathcal{G}}| + |V_G| - 1 = B_{\mathcal{G}} - \sum_{B \in B_{\mathcal{G}}} g_B$.

This is only a very rough estimate of the behavior of this integral. In fact, it is easy to see that if one can isolate a bubble of genus g from the others, then it carries a summation $\sum_j d_j^{2(1-g)} = \int \prod da_i db_i \delta^{\Lambda}(\prod_{i=1}^{g} [a_i, b_i])$. Thus the spherical bubbles contribute more than the toric bubbles while an isolated genus $g > 1$ bubble gives a convergent contribution.

Our goal is now to devise a new criterion analogous to the criterion of planarity in 2D GFT models or in matrix models that allow one to identify a subclass of graphs which dominates the contribution of the path integral in the limit of large spins.

Let us take a step back and revise the similar problem in matrix models [9]. Suppose that we start with the naive action

$$S = \frac{1}{2} \mathrm{Tr} H^2 + \frac{\lambda}{4} \mathrm{Tr} H^4, \tag{11}$$

for H some Hermitian $\Lambda \times \Lambda$ matrix. For a given graph $\mathcal{G}$, denote n, l, f its numbers of vertices, lines, and faces. Its amplitude is

$$A_{\mathcal{G}} = \lambda^n \Lambda^f. \tag{12}$$

As this amplitude is not uniform in the number of internal vertices, one could naively conclude that no renormalization transformation can be defied for a matrix model.

However this is known to be false. If one wishes to obtain a uniform power counting, not depending on the number of internal vertices, one needs to consider a rescaling of the coupling constant by some power of the cutoff

$$\lambda \to \frac{\lambda'}{\Lambda^{\alpha}}. \tag{13}$$

In order to determine the appropriate rescaling power α, recall that there exists a family of graphs for which a contraction procedure can be defined: the planar graphs. The combinatorics of the amplitude subtraction of a renormalization transformation can only be satisfied by this family.

The lowest order planar graph reproducing the vertex is made by two vertices connected by two lines and two lines which trap an internal face. It has amplitude $\lambda^2 \Lambda$. Requiring that the graph $\mathcal{G}$ and all the graphs where some of its vertices have been replace by such lowest order planar insertions have the same behavior with the cutoff, one determines the appropriate power α

$$\frac{\lambda'}{\Lambda^{\alpha}} = \frac{\lambda'^2}{\Lambda^{2\alpha}} \Lambda \Rightarrow \alpha = 1. \tag{14}$$

A posteriori one notes that after rescaling, $\mathcal{A}_{\mathcal{G}} = \lambda'^n \Lambda^{n-f} = \lambda'^n \Lambda^{2-2g}$, hence the planar graphs truly dominate the partition function.

The situation is more involved in 3D GFT. Still, one can start by looking for a family of graphs for which a contraction procedure can be defined. Once such a family is identified, by appropriately choosing a rescaling, one can presumably construct a model where such graphs dominate. The family of contractible graphs, also called type 1, is defined below and thoroughly analyzed in the rest of our paper.

Let b be a 2D connected component of the 2D projected graph $\bar{\mathcal{G}}$, and let $\mathcal{G}^b$ the 3D graph formed by the 3D ancestors of all its vertices and lines and $\bar{\mathcal{G}}^b$ the 2D the projection of $\mathcal{G}^b$.

Definition 1.—A graph $\mathcal{G}$ is called type 1 if

(1) $\forall$ b, any 3D vertex of $\mathcal{G}^b$ (and consequently 3D line or 3D face) projects into a *unique* 2D vertex (line or face) of b.

(2) For all b_1, there exists an ordering $b_1 < b_2 \ldots < b_{|B_{\mathcal{G}}|}$ such that

(a) $b_i \cap \bar{\mathcal{G}}^{b_1 \cup \ldots \cup b_{i-1}}$ is connected, for all $i \leq |B_{\mathcal{G}}|$.

(b) b_i is not contained in $\bar{\mathcal{G}}^{b_1 \cup b_2 \ldots \cup b_{i-1}}$, for $i < |B_{\mathcal{G}}|$.

We refer to the ordering $b_1 < b_2 < \ldots < b_{|\mathcal{B}_{\mathcal{G}}|}$ as the ordering associated to b_1. We sometimes refer to a graph which is not type 1 as a type 2 graph.

In a later section we establish the result.

Theorem 1.—The amplitude of a connected type 1 *manifold* vacuum 3D graph $\mathcal{G}$ is

$$A_{\mathcal{G}} = \lambda^{|V_{\mathcal{G}}|} (\delta^{\Lambda}(\mathbb{I}))^{|B_{\mathcal{G}}|-1}. \tag{15}$$

Both conditions in definition 1 enter crucially in our proof. Furthermore, the result is achieved by a complete contraction procedure. In this sense, the type 1 graphs are the family of contractible graphs. Any renormalization transformation must subsequently subtract only type 1 graphs.

We note that again, for the naive 3D GFT model, the degree of divergence is not uniform in the number of internal vertices. Inspired by the previous discussion on matrix models, we look for some rescaling of the coupling constant which presumably would render this degree of divergence uniform.

To find the appropriate power of the rescaling, we consider the first type 1 graph reproducing a vertex. It is the graph depicting a one to four topological move on the vertex. Its amplitude is $\lambda^4\delta(\mathbb{I}) \approx \lambda^4\Lambda^3$. Requiring again that the degree of divergence of a graph is invariant under substituting any vertex with this lowest order type 1 insertion yields

$$\frac{\lambda'}{\Lambda^\alpha} = \frac{\lambda'^4}{\Lambda^{4\alpha}}\Lambda^3 \Rightarrow \alpha = 1. \tag{16}$$

A posteriori we note that after rescaling the amplitude of a type 1 graph is $A_{\mathcal{G}} = \lambda'^{|V_{\mathcal{G}}|}\Lambda^{-|V_{\mathcal{G}}|+3(B_{\mathcal{G}}|-1)}$.

For this scaling limit to exist and behave in a similar way to that of our previous toy model, the following conjectures (amply verified on examples) must hold.

Conjecture 1.—At fixed order of perturbation, the number of bubbles $|B_{\mathcal{G}}|$ is maximal for type 1 graphs, and strictly smaller for all other graphs. If this holds, then the type 1 graphs dominate the partition function.

Conjecture 2.—At large order of perturbation, the number of bubbles of a type 1 graph with no two point subgraphs scales like $|V_{\mathcal{G}}|/3$. This would in turn ensure that the degree of divergence of type 1 graphs is uniform in the number of internal vertices.

Moreover, although not necessary from the point of view of field theory, we have also found the following natural conjecture to hold on all examples.

Conjecture 3.—Type 1 graphs are manifolds of trivial topology, i.e., isomorphic to the three-sphere.

The first two conjectures should hold due to the following. We will define a contraction procedure for 3D graphs. This procedure merges all the bubbles of a graph by iterated contractions and deletions of 3D lines. The contraction/deletion always exhausts the bubbles of a graph. What makes the type 1 graphs special is that the contraction/deletion furthermore exhausts all the 3D vertices of the graph. As we consider only graphs with no two point insertions, for any bubble there exist at least four 3D vertices which have descendents on it. Upon reduction, the number of 3D vertices diminishes then by at least three for every 3D bubble (as all 3D vertices having descendents on the bubble are contracted into one). Therefore $|B_{\mathcal{G}}| \leq |V_{\mathcal{G}}|/3$ and the bound is saturated for type 1 graphs.

Note that the definition of a type 1 graph is combinatorial and it can be easily extended to 4D and 2D GFTs. The 2D case is presented at length in Sec. IV below. For the 4D case, one can again define a complete contraction procedure and explicitly compute the amplitude of type 1 graphs. As this contraction is the crux of renormalization we presume that the type 1 graphs should play the crucial role of primitively divergent subgraphs also in that case. However, the amplitudes in 4D are more involved and a possible scaling limit is less clear. We therefore postpone the detailed generalization of our results to the 4D case for future work.

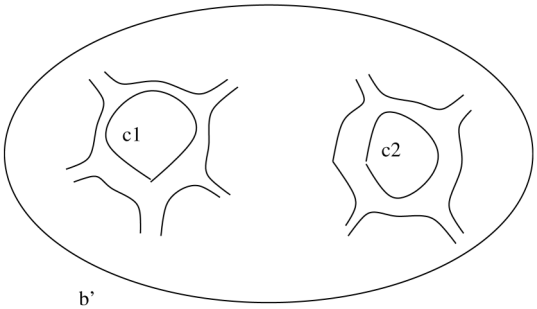

FIG. 9. A typical set of faces of b having common 3D ancestors with the faces of b'.

Returning to the 3D case, a final, technical point in this section is the following important property of type 1 graphs, called the property "P."

Definition 2.—A graph is said to have the property P if for any two bubbles b and b' of $\mathcal{G}$, the graph $\bar{\mathcal{G}}^b \cap b'$ is such that *any two faces* (that is closed strands) do *not share* the same line.

Before proceeding we will prove the lemma.

Lemma III.1.—Type 1 graphs obey the property P.

The proof is very simple and relies basically only on the analysis of Fig. 5. What we will see in the following is that there exists graphs which satisfy the property P but are not of type 1, so these two conditions are not equivalent.

Proof.—By the first hypothesis of being of type 1, the 2D vertices $(1_2, 1_3, 1_4)$ and $(2_1, 2_3, 2_4)$ have to belong to two distinct bubbles, say b and b'. They share the descendants 1_2 and 2_1 of the strand (1, 2). Consequently $\bar{\mathcal{G}}^b \cap b'$ contains the whole face 2_1 (and symmetrically $\bar{\mathcal{G}}^{b'} \cap b$ contains 1_2). On the contrary, the faces 1_3 and 1_4 are shared by 1 and 3 and 1 and 4. But each of 1, 2, 3, and 4 belong to a different bubbles, as the graph is type 1. Hence the bubbles b and b' share just one face coming from the vertex (1, 2, 3, 4), and none of its neighbors. As this is true for any vertex, the two bubbles will share a set of faces not neighboring each other (that is, not sharing any lines).

This is represented in Fig. 9.

We will see later on that this property is a crucial ingredient of the contraction procedure we define for type 1 graphs, and thus for our main result concerning the power counting for the same class of graphs.

IV. TYPE 1 GRAPHS IN TWO DIMENSIONS

Before addressing the three-dimensional case we will detail the two-dimensional type 1 graphs. The importance of this study is twofold. First, we will show that these

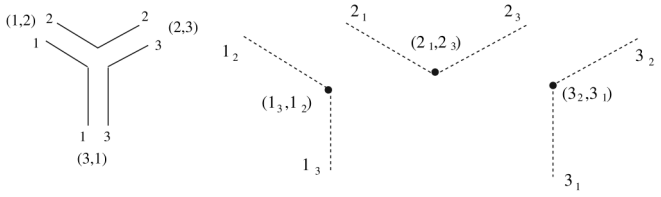

FIG. 10. Two neighboring faces.

graphs in two dimensions are exactly planar, one particle irreducible graphs, thus strengthening our claim that the type 1 graphs are dominant in three dimensions. Second, the proof relies on a contraction/deletion technique, similar to that of [24] which is then generalized and applied to our results in three dimensions.

We start by generalizing the projection in a straightforward way to two-dimensional graphs, as shown in Fig. 10. The two-dimensional vertex (1, 2, 3) projects into *three* one-dimensional vertices $(1_3, 1_2)$, $(2_1, 2_3)$, and $(3_2, 3_1)$, represented by dots in Fig. 10. Each two-dimensional half-line projects into *two* one-dimensional half-lines; (1, 2) for instance projects into 1_2 and 2_1. The two-dimensional bubbles are the faces of the graph, hence we denote them as $F \in \mathcal{F}$. Each of them projects into *one* one-dimensional connected component, f. Note that the 1D graphs (the connected components corresponding to the bubbles) obtained by projection are particularly trivial: they are cycles of lines and vertices of coordination two. The property P, for instance, translates trivially for two-dimensional graphs as:

Definition 3.—A two-dimensional graph $\mathcal{G}$ is said to have the property P if for any two faces f and f' of $\mathcal{G}$ the graph $\bar{\mathcal{G}}^f \cap f'$ are such that any two lines do not share a vertex.

Here we used again the notation $\bar{\mathcal{G}}^f$ for the 1D projection of the 2D ancestor of the face f. One can also translate the definition of type 1 graphs as:

Definition 4.—A graph $\mathcal{G}$ is called type 1 if

(1) $\forall$ f, any 2D vertex of $\mathcal{G}^b$ (and consequently 2D line) projects into an unique 1D vertex (or line) of f.
(2) For all f_1, there exists an ordering $f_1 < f_2 \ldots < f_{|F_\mathcal{G}|}$ such that
(a) $f_i \cap \bar{\mathcal{G}}^{f_1 \cup \ldots \cup f_{i-1}}$ is connected, for all $i \leq |F_\mathcal{G}|$.
(b) f_i is not contained in $\bar{\mathcal{G}}^{f_1 \cup f_2 \ldots \cup f_{i-1}}$ for $i < |B_\mathcal{G}|$.

Unsurprisingly, the type 1 graphs have the property P. The first condition of type 1 implies that the three faces meeting at any two-dimensional vertex are distinct, thus $1 \neq 2 \neq 3 \neq 1$ in Fig. 10. Hence, any pair of neighboring lines like (1, 2) and (1, 3) can never be shared by the same two faces.

Generically, a 2D line L separates two different faces. If one of these two faces is bounded *only* by the line L (as is for instance the case for a planar tadpole), we will call the latter a "simple line."

In 2D there exist two topological "moves," [24] which allow one to reduce a graph to an irreducible, topological equivalent one. These two moves are the contraction of a 2D tree line and the deletion of a 2D simple line. The topology of an orientable 2D graph is entirely encoded in its Euler character, $2 - 2g = V - L + F$. The deletion of a tree line reduces both the number of vertices and lines by 1, while the deletion of a simple line reduces both the number of lines and faces by 1. The Euler character is thus invariant under this move, and subsequently the amplitude (in the scaling limit) is unchanged. However, the valence of the vertices of the graph changes. The graphs obtained by applying this simplification will no longer be dual to simplicial complexes, but to more general cellular complexes.

A natural question arises. Given a 2D graph $\mathcal{G}$, what is the effect of the 2D topological moves on its 1D projection $\bar{\mathcal{G}}$?

In order to answer this question, let us consider a 2D line L, connecting the two 2D vertices V and V' and separating two[3] faces F_1 and F_2. The two faces F_1 and F_2 project into two connected components f_1 and f_2, the line L projects into two 1D lines $l_1 \in f_1$ and $l_2 \in f_2$ and the vertices V and V' project into the 1D vertices v_1, $v_1' \in f_1$ and v_2, $v_2' \in f_2$. l_1 connects v_1 and v_1' while l_2 connects v_2 and v_2'.

First, let L be a 2D tree line, that is $V \neq V'$. Consequently $v_1 \neq v_1'$ and $v_2 \neq v_2'$. The contraction of the 2D line L (and the gluing of vertices V and V') projects into the contraction of the line l_1 (and gluing of v_1 and v_1') in b_1, accompanied by the contraction of l_2 (and gluing of v_2 and v_2') in b_2. Now suppose that L is a simple line. Take f_1 the connected component formed only by the line l_1, that is $v_1 = v_1'$. The deletion of the line L projects in the deletion of the 1D connected component f_1 accompanied by the *contraction* of the 1D line l_2 in f_2, (and the gluing of v_2 and v_2').

We are now in the position to state the main result of this section.

Theorem 2.—A 2D graph $\mathcal{G}$ is type 1 if and only if it is a planar one particle irreducible graph.

Proof.—The idea of the proof is simple. We will first show that the total order associated to f_1 specifies a sequence of topological moves which ultimately reduce the graph to a planar tadpole. Conversely, for a planar graph one can always chose a sequence of moves which reduce it to a planar tadpole. This sequence of moves will in turn uniquely define a total order for its faces. The detailed (somewhat technical) proof is presented below.

Let $\mathcal{G}$ be a type 1 graph.

Suppose that $\mathcal{G}$ is a one particle reducible graph. The reducibility line L, connecting the vertices V_1 and V_2 separates the 2D graph into two connected components

[3]These two faces are not necessarily distinct.

$\mathcal{C}_1 \ni V_1$ and $\mathcal{C}_2 \ni V_2$. The subgraph $\mathcal{C}_1$ would have only one face broken by L, say F. Consequently, the vertex V_1 would have two 1D descendents in the connected component f, the projection of F. As this violates the first condition in definition 4, we conclude that $\mathcal{G}$ is one particle irreducible.

Now take the first connected component f_1 in the order specified in definition 4. Denote the 1D vertices of f_1 by $v_1, \ldots, v_p$. Each of them descends from different 2D vertices $V_1, \ldots V_p$ belonging to the 2D ancestor F_1 of f_1. Consider all lines save one of f_1, $l_1 = (v_1, v_2), \ldots l_{p-1} = (v_{p-1}, v_p)$, and their 2D ancestors, $L_1 = (V_1, V_2), \ldots L_{p-1} = (V_{p-1}, V_p)$. As the projection is one to one and $l_1, \ldots l_{p-1}$ do not form a loop, $L_1, \ldots L_{p-1}$ do not form a loop either. As such they are tree lines and can be contracted. After contraction f_1 has become a 1D connected component with only one vertex and one line l_p. Its 2D ancestor L_p is then simple, and can be deleted. This shows that we can contract and delete f_1

The contraction/deletion of the component f_1 *contracts* each $f_k \cap \bar{\mathcal{G}}^{f_1}$ in a unique 1D vertex. In particular, in the component f_2, the connected subgraph $f_2 \cap \bar{\mathcal{G}}^{f_1}$ has been contracted to a unique vertex. Thus, for f_2, each of its 1D vertices will still have a unique 2D ancestor. The ancestor of a tree in f_2 is still a set of tree lines in $\mathcal{G}$, and thus we can iterate the procedure. Ultimately we exhaust all but one 2D line. The final graph will have one vertex and one loop line and consequently is a planar tadpole graph. Hence $\mathcal{G}$ is a planar graph.

Let $\mathcal{G}$ be a planar, 1PI graph.

Suppose there exists a 2D line L, with both strands belonging to the same face. For instance, suppose that $1 = 2$ in Fig. 10. As $\mathcal{G}$ is 1PI, we can always contract a maximal tree[4] *not* containing L. After contraction, the graph $\mathcal{G}$ becomes a rosette.[5] On this rosette the two sides of L are the same face and there must exist some other line, L', connecting them. The two lines L and L' generate a crossing on the rosette which contradicts the hypothesis that $\mathcal{G}$ is a planar.

Thus, all 2D lines L must separates two different faces. This implies that for trivalent[6] vertices (see Fig. 10) the three descendents of the vertex belong to the distinct connected components. Hence the first condition of definition 4 holds.

We will now construct a total order on the connected components f respecting the conditions stated in 4. Chose any face, say F_1 and denote its projection f_1 as the first in the order. We will prove that, because $\mathcal{G}$ is planar, there always exists a face, F_2, sharing exactly one line with F_1. We set its projection f_2 as the successor of f_1 in the total order. For two faces F_1 and F_2 sharing exactly one line $L = (V, V')$, we construct the face $(F_1 \sqcup_L F_2)$ by deleting the line L *and* the vertices V, V'; see Fig. 11. Consequently the lines L_1, L_2 and L_1', L_2' are joint into new lines $(L_1 \sqcup L_2)$ and $(L_1' \sqcup L_2')$. In short we obtain by deleting the line L a new planar graph which is one particle irreducible, whose face is either an initial face or the "new face" $(F_1 \sqcup_L F_2)$ and similarly edges are either initial edges or the new edges $(L_1 \sqcup L_2)$ and $(L_1' \sqcup L_2')$. Since this graph satisfies our initial hypothesis, we can find a face F_3 sharing only one edge with the face $(F_1 \sqcup_L F_2)$ and continue recursively the procedure till exhaustion of the faces. By iteration we obtain a total order of the faces of the graph, respecting the requirements of definition 4, thus proving that $\mathcal{G}$ is a type 1 graph.

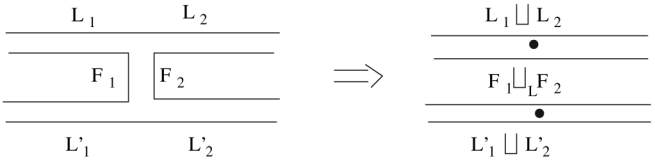

FIG. 11. The joining of two faces separated by one line, $F_1 \sqcup_L F_2$.

To conclude we just need to prove that for any face F_1 of a planar graph there exists a face F_2 sharing exactly one line with it. Let F a face sharing at least a 2D line with F_1. Suppose F_1 and F share two lines, say at least two lines, we take L_1 and L_2 to be two consecutive such lines as in Fig. 12. Note that L_1 and L_2 cannot touch the same 2D vertex because the vertices are trivalent, and the three descendents of a vertex belong to different connected components. This shows that there exists lines $L_a, \ldots$ between L_1 and L_2, encompassed by the face F like in Fig. 12. Take the face F_a which shares the line L_a with F_1. If F_a shares only one line then we are done. Otherwise F_a and F_1 share two consecutive lines, L_a and L_b. As the graph is planar, no line can intersect the dotted circuit in Fig. 12, hence L_b must also be between L_1 and L_2. We then chose F_a instead of F and repeat the argument. We will

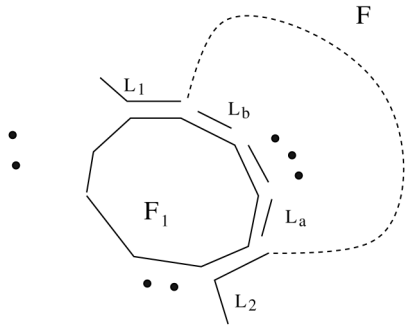

FIG. 12. Two faces, F_1 and F, that share two lines in a planar graph.

[4]A tree connecting all vertices of the graph $\mathcal{G}$.
[5]A graph with only one 2D vertex.
[6]This does not hold for four valent vertices as the reader can easily check.

always end up with a face F_2 which will share exactly one line with F_1. ■

V. EXAMPLES OF GRAPHS

In this section we will present some 3D graphs, identify their 2D projections, and compute their amplitudes. For simplicity we only consider vacuum graphs.

A. A type 1 manifold graph

Our first example is the graph $\mathcal{G}_1$ presented together with its bubbles in Figs. 7 and 8 at the end of Sec. III A. We denote the four connected components of the 2D projection $\bar{\mathcal{G}}$ in Fig. 8 by $b_1 = (l_1, l_2, l_3)$, $b_2 = (l_1, l_3, l_4)$, $b_3 = (l_1, l_2, l_4)$, and $b_4 = (l_2, l_3, l_4)$.[7] The relation between the topological numbers of the graph $\mathcal{G}_1$ and those of the graph $\bar{\mathcal{G}}_1$ can be directly verified. Thus, for instance, the 2D descendents of the 3D line L_1 belong to the components b_1, b_2, and b_3 whereas the 2D descendants of the face (L_1, L_2) belong to the b_1 and b_3.

In this particular case, all the bubbles b_1, b_2, b_3, and b_4 are planar (spheres), hence the graph $\mathcal{G}_1$ represents a manifold. We can check for this particular graph that both conditions in definition 1 are fulfilled. Therefore $\mathcal{G}_1$ is a type 1 graph.

This graph is typical for the class of graphs for which we will establish the power counting in Sec. VI. Therefore, at the risk of being slightly pedantic, we will treat it in great detail in this section, so to give a good feeling of the general contraction procedure, and of the origin of the power counting result. The task is, briefly, to identify some combinatorial substructure in the graph, which implies that the corresponding group elements can be easily integrated out in evaluating the amplitudes. Then we need to perform the relative integrations and obtain a general factorization property for the elements in the amplitude that correspond to the connected components of $\bar{\mathcal{G}}$, thus to the bubbles of the 3D graph $\mathcal{G}$, which is where the divergences of the model reside. We start by orienting all lines from the vertex $V = (1, \ldots 12)$ to the vertex $V' = (1', \ldots 12')$. Denoting the group elements associated to the 3D lines of the graph by $h_{L_1}, \ldots h_{L_4}$, the amplitude of $\mathcal{G}_1$ is

$$A_{\mathcal{G}_1} = \int dh_{L_1} dh_{L_2} dh_{L_3} dh_{L_4} \delta^\Lambda(h_{L_1} h_{L_2}^{-1}) \delta^\Lambda(h_{L_1} h_{L_3}^{-1}) \times \delta^\Lambda(h_{L_1} h_{L_4}^{-1}) \delta^\Lambda(h_{L_2} h_{L_3}^{-1}) \delta^\Lambda(h_{L_2} h_{L_4}^{-1}) \delta^\Lambda(h_{L_3} h_{L_4}^{-1}). \tag{17}$$

Step 1.—Contraction of a tree in b_1. We choose the line l_1 which is a tree line in the component b_1 (actually, in this specific example, it corresponds to a full tree in b_1). We associated two group elements, g_V and $g_{V'}$, to the vertices V and V', respectively. We make the change of variables

$$\begin{aligned} h_{L_2} &= g_V^{-1} h'_{L_2} g_{V'} \qquad & h_{L_3} &= g_V^{-1} h'_{L_3} g_{V'} \\ h_{L_4} &= g_V^{-1} h'_{L_4} g_{V'} \qquad & h_{L_1} &= g_V^{-1} g_{V'}. \end{aligned} \tag{18}$$

Now we choose one group element g_V among those appearing in the amplitude and we keep it fixed while computing the other integrations; this is the group element associated to the root of the tree we are considering. We get (neglecting the primes)

$$A_{\mathcal{G}_1} = \int dg_{V'} dh_{L_2} dh_{L_3} dh_{L_4} \delta^\Lambda(h_{L_2}^{-1}) \delta^\Lambda(h_{L_3}^{-1}) \delta^\Lambda(h_{L_4}^{-1}) \times \delta^\Lambda(h_{L_2} h_{L_3}^{-1}) \delta^\Lambda(h_{L_2} h_{L_4}^{-1}) \delta^\Lambda(h_{L_3} h_{L_4}^{-1}). \tag{19}$$

We then see that the integral over g_V gives 1, as g_V itself has disappeared from the amplitudes and the Haar measure is assumed to be normalized.

The remaining integrals in Eq. (19) correspond to a graph, (denoted by $\mathcal{G}'_1$) obtained from $\mathcal{G}$ by contracting the line L_1. Consequently the 2D projection of $\mathcal{G}'_1$, denoted by $\bar{\mathcal{G}}'_1$, is obtained from Fig. 8 by contracting the lines l_1 (see Fig. 13).

We denote the connected components of $\bar{\mathcal{G}}'_1$ by $b'_1 = (l_2, l_3)$, $b'_2 = (l_3, l_4)$, $b'_3 = (l_2, l_4)$, and $b'_4 = (l_2, l_3, l_4)$. The component b'_1, obtained from b_1 by contracting l_1 is called a "rosette," a graph topologically equivalent to b_1 but with only one vertex; the topological equivalence of the two graphs is easily verified as the contraction eliminates at once a line and a vertex, thus keeping the genus of the corresponding two-surface invariant.

Step 2.—Integration of all but one loop line of b_1. All the delta functions in Eq. (19) correspond to faces of $\mathcal{G}'_1$, hence they have two descendents in $\bar{\mathcal{G}}'_1$. Like the original graph, the two descendents of a 3D face belong to two distinct connected components, and any two connected components share the 2D descendents of at most one 3D face.

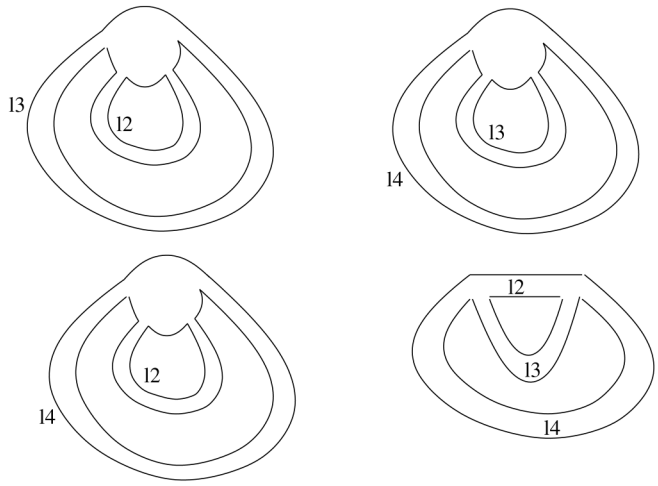

FIG. 13. The graph $\bar{\mathcal{G}}'_1$.

[7] We do not distinguish between the 2D descendents of the same 3D line so not to make the drawings overly involved.

This follows from the very definition of type 1 graphs. For instance, the 2D descendents of the 3D face $\delta(h_{L_2}^{-1})$ belong to b_1' and b_3' while those corresponding to $\delta(h_{L_3}^{-1})$ belong to b_1' and b_2'.

b_1' is a planar graph and has only one vertex. In consequence, the loop lines do not cross. Consider the face bounded only by l_2 of b_1'. We integrate the group element h_{L_2} using $\delta(h_{L_2}^{-1})$. Thus (19) becomes

$$A_{\mathcal{G}_1} = \int dh_{L_3} dh_{L_4} \delta^\Lambda(h_{L_3}^{-1}) \delta^\Lambda(h_{L_4}^{-1}) \delta^\Lambda(h_{L_3}^{-1}) \delta^\Lambda(h_{L_4}^{-1}) \times \delta^\Lambda(h_{L_3} h_{L_4}^{-1}). \tag{20}$$

The line l_2 appeared in three instances in the graph $\bar{\mathcal{G}}_1'$: twice as a loop line (on b_1' and b_3') and once as a tree line (on b_4'). The integration of h_{L_2} has as consequence to delete l_2 each time it appeared as a loop line, but to *contract* it where it appeared as a tree line. Thus the new expression (20) corresponds to the reduced graph $\bar{\mathcal{G}}_1''$ presented in Fig. 14. For more complicated graphs, we would repeat the procedure for all the lines forming our tree.

Step 3.—Factorization of b_1 using the last loop line. The connected components of $\bar{G}''$ are denoted $b_1'', \ldots b_4''$. b_1'' has only one surviving loop line. It has two faces with amplitude $\delta(h_{L_3}^{-1})$. We call f_1 the exterior face and f_2 the interior one in Fig. 14. The two faces cannot be descendents of the same 3D face (as the descendents belong to different bubbles, because of the type 1 condition). In fact the copy of the interior face f_2 (called $\tilde{f}_2$) belongs to the bubble b_4'', while the copy of the exterior face f_1 (called $\tilde{f}_1$) belongs to b_2''.

We conclude that $\delta(h_{L_3}^{-1})$ appears twice in the expression of the amplitude [as can be checked directly on Eq. (20)]. This implies that all the 2D descendents l_3 of L_3 are loop lines, belonging to different bubbles.

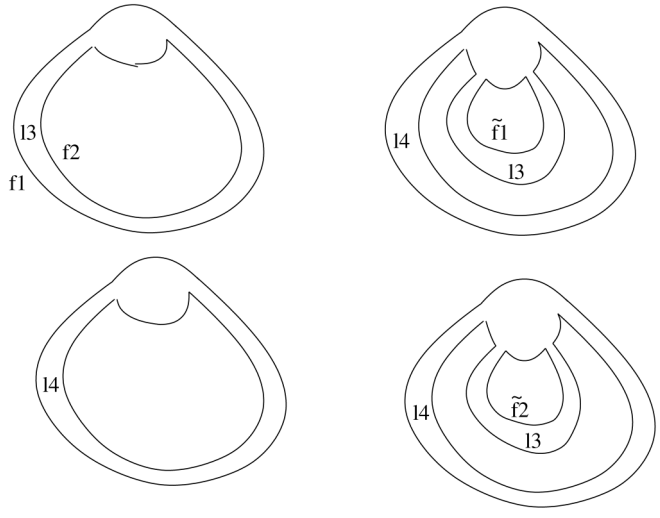

FIG. 14. The graph $\bar{\mathcal{G}}_1''$.

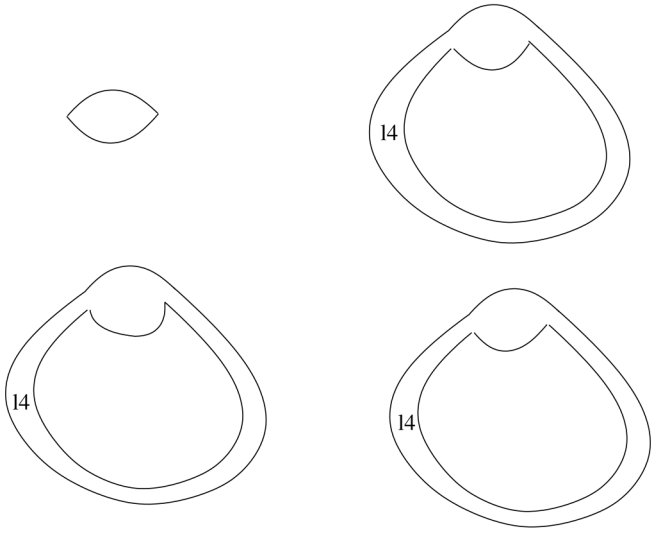

FIG. 15. The graph $\bar{\mathcal{G}}_1'''$.

We integrate $h_{L_3}^{-1}$. The amplitude becomes

$$A_{\mathcal{G}_1} = \delta^\Lambda(\mathbb{I}) \int dh_{L_4} \delta^\Lambda(h_{L_4}^{-1}) \delta^\Lambda(h_{L_4}^{-1}) \delta^\Lambda(h_{L_4}^{-1}). \tag{21}$$

It corresponds to the graph $\bar{\mathcal{G}}_1'''$ obtained from $\bar{\mathcal{G}}_1''$ by deleting all the 2D descendents l_3 of L_3 (see Fig. 15).

We are now in the situation where the only surviving 2D lines l_4 are all descendents of the same 3D line L_4. They belong to three distinct bubbles. Integrating h_{L_4} yields

$$A_{\mathcal{G}_1} = [\delta^\Lambda(\mathbb{I})]^3. \tag{22}$$

This is the final result for the amplitude. It corresponds to having, in absence of the cutoff we imposed for regularizing the Feynman amplitudes of our model, one delta function divergence for each bubble (which has necessarily a boundary of spherical topology, as we assumed $\mathcal{G}$ to be a manifold) in the 3D graph $\mathcal{G}$, and with an amplitude that is completely factorized per bubble.

B. A type 2 manifold graph

We now consider a similar graph, obtained from the previous one by a simple change in the gluing of the two GFT vertices it is composed of. The change amounts to an exchange between two of the lines of propagation, but is has the important consequence of violating the first type 1 condition: one of the faces in the projected graph $\bar{\mathcal{G}}$ in fact appears twice in the same bubble. As in this subsection and in the next we will simply compute the amplitudes without detailing the various steps of the computation; we will not use distinct letters for the 3D lines and there 2D descendents.

Consider now the graph $\mathcal{G}_2$, depicted in Fig. 16. Its bubbles are once more easily identified and are drawn in Fig. 17.

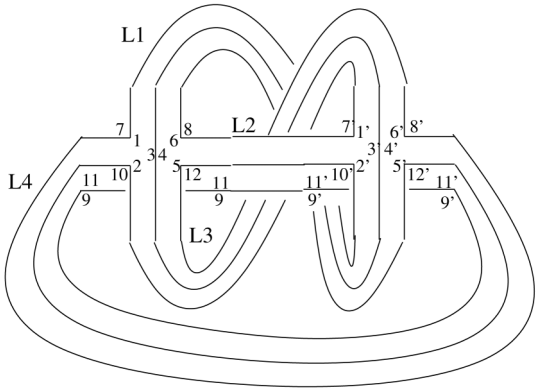

FIG. 16. The twisted sunshine graph $\mathcal{G}_2$.

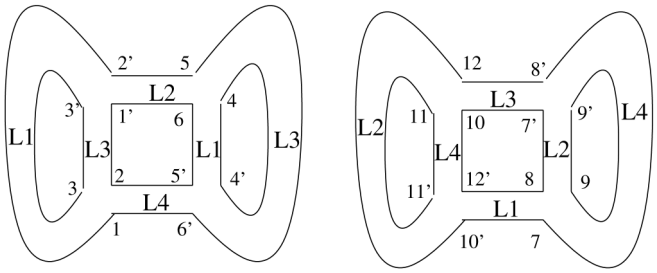

FIG. 17. Bubbles of the graph $\mathcal{G}_2$ (the graph $\bar{\mathcal{G}}_2$).

First of all, notice that, as the boundaries of the two bubbles are both two-spheres, this graph represents a manifold just as the previous example we considered. Unlike the previous example, however, as we noted, the face (L_1, L_2) appears twice on the same bubble hence it is a type 2 graph. However, as we will see, this manifold is such that its first homotopy group is nontrivial that is $\Pi_1(M) = \mathbb{Z}_2$; it is therefore not a three-sphere. This is consistent with our conjecture that all type 1 graphs are manifolds of trivial topology.

The amplitude of this graph is given by

$$A_{\mathcal{G}_2} = \int dh_{L_1} dh_{L_2} dh_{L_3} dh_{L_4} \delta^\Lambda(h_{L_1} h_{L_2}^{-1} h_{L_3} h_{L_4}^{-1}) \times \delta^\Lambda(h_{L_1} h_{L_3}^{-1}) \delta^\Lambda(h_{L_1} h_{L_4}^{-1} h_{L_3} h_{L_2}^{-1}) \delta^\Lambda(h_{L_2} h_{L_4}^{-1}) \quad (23)$$

and using the same change of variables as in Eq. (18) it becomes

$$\begin{aligned} A_{\mathcal{G}_2} &= \int dh_{L_1} dh_{L_2} dh_{L_3} dh_{L_4} \delta^\Lambda(h_{L_2}^{-1} h_{L_3} h_{L_4}^{-1}) \delta^\Lambda(h_{L_3}^{-1}) \times \delta^\Lambda(h_{L_4}^{-1} h_{L_3} h_{L_2}^{-1}) \delta^\Lambda(h_{L_2} h_{L_4}^{-1}) \\ &= \int dh_{L_2} dh_{L_4} \delta^\Lambda(h_{L_2}^{-1} h_{L_4}^{-1}) \delta^\Lambda(h_{L_4}^{-1} h_{L_2}^{-1}) \delta^\Lambda(h_{L_2} h_{L_4}^{-1}) \\ &= \delta^\Lambda(\mathbb{I}) \int dh_{L_2} \delta^\Lambda(h_{L_2}^{-1} h_{L_2}^{-1}), \end{aligned} \quad (24)$$

where in the last equality we have given the dominant divergent contribution in the large Λ limit. The last integration can easily be performed in the $SO(3)$ case, for example, giving a divergent (in absence of regularization) contribution of the form $\sum_{n\in\mathbb{N}}(2n+1)$. As we will see later on, the failure to satisfy the type 1 conditions prevents the power counting formula we prove in this work to be satisfied. It shows that power counting is not uniform in the number of vertices so that, if type 1 graphs can be made to dominate over type 2 graphs, this has to be in some scaling limit. One sees however that for a given order in perturbation theory the type 1 graph is the most divergent, having more bubbles.

C. A type 2 pseudomanifold graph

As our last example, we now consider another variation of the same two-vertex graph. This time, we add a further exchange in the gluing of the two vertices. This has both the consequences that the resulting cellular complex fails to satisfy the type 1 conditions, and it also fails to satisfy the manifold conditions, since once of its bubbles has the topology of a torus, as it can be easily checked. Moreover this graph possess two bubbles which share only one face, thus the graph satisfies the property P even if it is not type 1. Our third graph, called $\mathcal{G}_3$ and its bubble $\bar{\mathcal{G}}_3$ are drawn in Figs. 18 and 19, respectively.

The amplitude associated to $\mathcal{G}_3$ is

$$A_{\mathcal{G}_3} = \int dh_{L_1} dh_{L_2} dh_{L_3} dh_{L_4} \delta^\Lambda(h_{L_1} h_{L_2}^{-1} h_{L_4} h_{L_1}^{-1} h_{L_2} h_{L_4}^{-1}) \times \delta^\Lambda(h_{L_1} h_{L_3}^{-1} h_{L_4} h_{L_3}^{-1}) \delta^\Lambda(h_{L_2} h_{L_3}^{-1}) \quad (25)$$

which rewrites using again Eq. (18) as

$$A_{\mathcal{G}_3} = \int dh_{L_2} dh_{L_3} dh_{L_4} \delta^\Lambda(h_{L_2}^{-1} h_{L_4} h_{L_2} h_{L_4}^{-1}) \delta^\Lambda(h_{L_3}^{-1} h_{L_4} h_{L_3}^{-1}) \times \delta^\Lambda(h_{L_2} h_{L_3}^{-1}) \int dh_{L_2} dh_{L_4} \delta^\Lambda(h_{L_2}^{-1} h_{L_4} h_{L_2} h_{L_4}^{-1}) \times \delta^\Lambda(h_{L_2}^{-1} h_{L_4} h_{L_2}^{-1}). \quad (26)$$

The second delta function tells us that $h_{L_4} = h_{L_2}^2$ and substituting this in the first delta function yields

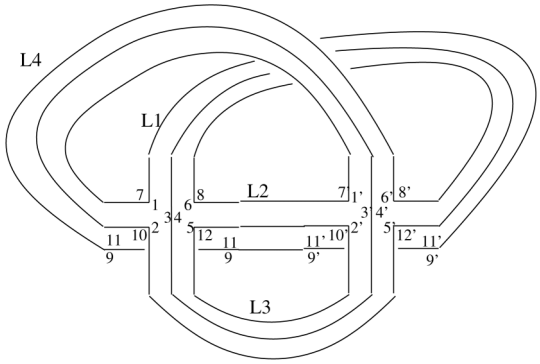

FIG. 18. The permuted sunshine graph $\mathcal{G}_3$.

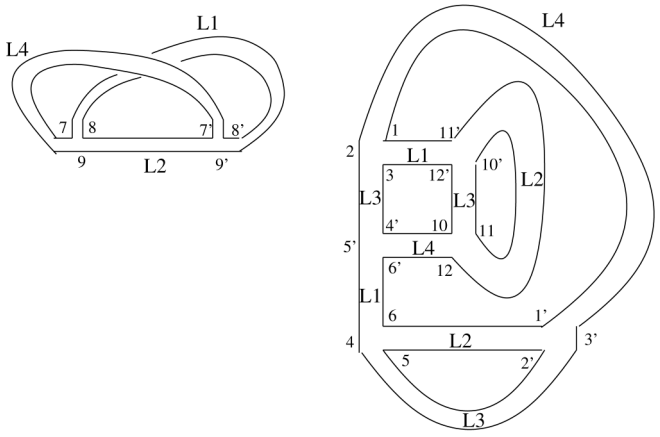

FIG. 19. Connected components associated to the bubbles of the graph $\mathcal{G}_3$ (the $\bar{\mathcal{G}}_3$ graph).

$$A_{\mathcal{G}_3} = \delta(\mathbb{I}) \int dh_{L_2} dh_{L_4} \delta^{\Lambda}(h_{L_2}^{-1} h_{L_4} h_{L_2}^{-1}) = \delta(\mathbb{I}). \quad (27)$$

We thus see that this graph has a divergence (in the absence of regularization) that is again of delta function type for each bubble of the graph minus one, as in the first example we have shown, and as our power counting theorem gives, in spite of the fact that, contrary to that example, it does not define a manifold. This implies that the topology of the cellular complex is reflected in the divergence of the amplitudes of the model in a way that is far from trivial. Also, this further example supports the conjecture that type 2 graphs are in general less divergent than type 1 graphs, at the same order in perturbation theory. This is further confirmed by all the examples we considered at higher (but still low) order.

VI. POWER COUNTING

In this section we will prove a power counting theorem for type 1 manifold graphs. The first part of our derivation can be applied, actually, to an arbitrary graph. It is only in the second part that the restriction to type 1 manifolds will play a role.

The idea of the proof is simple. We apply topological moves to the given graph $\mathcal{G}$ to obtain from it a second graph $\mathcal{G}'$, such that the quantum amplitudes of the two graphs are equal. Applying then a well-defined sequence of further moves, we simplify the graph $\mathcal{G}'$, and are in the end able to compute the amplitude. The point is that the topological moves used are devised in such a way that they not only simplify the graph, but also separate the contribution to the amplitude coming from the different bubbles. This sequence of topological moves is what we call a contraction process, which we highlight as the basis of the GFT renormalization procedure.

For simplicity we will restrict our attention to vacuum graphs. The generalization to graphs with arbitrary numbers of external legs is straightforward.

Before we proceed, we note here an important point of the construction. Our topological moves lead, from diagrams that are dual to simplicial complexes, i.e., the original GFT Feynman diagrams, to cellular complexes with more general combinatorics. Our construction therefore works and our theorem holds for a larger class of diagrams than those obtained from the Boulatov model. In other words, our results apply to any GFT model in three dimensions (i.e., with a field depending on three group arguments and still corresponding to a triangle) with trivial vertex and kinetic terms in the action (i.e., given by delta functions on the group), as in the Boulatov model, but with interaction terms of arbitrary order provided the identifications are still pairwise and the corresponding complexes are oriented (with outward triangle normals). Therefore, we consider a slightly larger category of graphs than those of the initial GFT, namely, the vertices in our 3D graphs have arbitrary coordination. The dual of such a vertex is a convex polyhedron with the boundary triangulated by triangle duals to the half-lines in the graph. Consequently the 2D graphs embedded in the 3D graph (the bubbles) will have vertices of arbitrary coordination as well. Notice that such a GFT model will have again Feynman amplitudes given by delta functions over the group, whose arguments will again be holonomies of an $SU(2)$ connection around a closed path encircling the 3D edges of a cellular complex; in other words, it will still correspond to a GFT quantization of 3D BF theory (and thus strictly related to 3D gravity), just like the simpler Boulatov model, now discretized on a more general cellular complex.

A. The contraction of a tree

We prove first a lemma stating the invariance of the GFT amplitudes for the class of models we consider under part of the contraction procedure for Feynman graphs we define.

Lemma VI.1.—The amplitude of a graph is invariant under the contraction of a 3D tree line.

Proof.—Consider an arbitrary graph $\mathcal{G}$, and choose a tree line L exiting from the vertex V_p and entering in the vertex V_q. To this tree line, one single group element h_L is associated, which will, by construction, be shared by three (not necessarily distinct) faces of the graph. We denote by $L_p \in V_p$ ($L_q \in V_q$) all other lines of $\mathcal{G}$ touching V_p (V_q). We now want to isolate and characterize, first, the contribution of this tree line to the full amplitude, and then check the effect of removing this line from the graph, by integrating it out. Let us focus on the faces of the graph. Looking at their relation with the tree line L, they can be classified in five distinct types:

(i) The face of type F_0 does not touch either of the vertices V_p or V_q.

(ii) The face of type F_1 goes from the vertex V_p, through the line L, to the vertex V_q.

(iii) The face of type F_2 goes from the vertex V_q, through the line L, to the vertex V_p.
(iv) The face of type F_3 touches the vertex V_p with two strands but does not cross over to the vertex V_q; therefore its boundary does not include the tree line L.
(v) The face of type F_4 touches the vertex V_q with two strands but does not cross over to the vertex V_p; therefore its boundary does not include the tree line L.

Clearly, the three faces whose boundaries includes the tree line L can only be of type F_1 or F_2, and the delta functions associated to these faces will of course contain the group element h_L, or its inverse h_L^{-1}, respectively, in their argument; so we can have three F_1 faces, three F_2 faces, or two faces of one type and one of the other. The effect of the contraction of the tree line L is different for the above five types of faces, and this is what we need to study here. We can highlight the contribution of the vertices V_p and V_q, touched by the tree line L, to the full amplitude $A_{\mathcal{G}}$ by writing the same amplitude as:

$$A_{\mathcal{G}} = \Big(\prod_l \int dh_l\Big)\prod_{F_0}\delta_{F_0}(\dots h_l \dots) I(h_l),$$

where l labels the lines of $\mathcal{G}$ that do not touch the vertices V_p and V_q, F_0 indicates the faces that only have such lines in their boundary, and I represents instead the contribution to the amplitude coming from the faces that touch the vertices V_q and V_p. This, we repeat, will be given by the three deltas associated to the three faces of type F_1 or F_2 and depending on h_L, times all the other deltas of type F_3 or F_4; all these deltas will *a priori* depend also on the group elements h_l. In order to simplify the exposition, we assume that at least one of the three faces depending on h_L is of type F_1 and at least one of them is of type F_2; we focus on these two faces and leave implicit the third one, because it will behave (under contraction of the tree line L), just as one of the other two. Similarly, we focus only on two of the faces of type F_3 and F_4, assuming that I contains at least one face of each type. Again, this simplifies the presentation and makes the proof of the lemma clearer, but the same reasoning would hold in the most general case as well. The contribution of L to the amplitude then writes

$$I(h_l) = \Big(\prod_{L_p\in V_p}\int dh_{L_p}\prod_{L_q\in V_q}\int dh_{L_q}\int dh_L\Big)\delta_{F_1}(\dots h_{L_{p_1}}^{\sigma(L_{p_1})} h_L h_{L_{q_1}}^{\sigma(L_{q_1})}\dots)\delta_{F_2}(\dots h_{L_{q_2}}^{\sigma(L_{q_2})} h_L^{-1} h_{L_{p_2}}^{\sigma(L_{p_2})}\dots)$$
$$\times\,\delta_{F_3}(\dots h_{L_{p_3}}^{\sigma(L_{p_3})} h_{L_{p_4}}^{\sigma(L_{p_4})}\dots)\delta_{F_4}(\dots h_{L_{q_3}}^{\sigma(L_{q_3})} h_{L_{q_4}}^{\sigma(L_{q_4})}\dots)\prod_F \delta_F(\dots.), \tag{28}$$

where F labels the other face of type F_1 or F_2 that we know is contributing to the amplitude, and all the other faces of type F_3 and F_4 that we do not focus on. The exponent $\sigma(L_{p_1})$ in δ_{F_1} is 1 if the orientation of the line L_p coincides with that of the face F_1 and -1 if not (and similarly for all other exponents).

Let us now associate two group elements g_{V_p} and g_{V_q} to the vertices V_p and V_q, and change variables as follows:

$$\begin{aligned} h_{L_p} &= h'_{L_p} g_{V_p} \text{ if } h_{L_p} \text{ enters in the vertex } V_p \\ h_{L_p} &= g_{V_p}^{-1} h'_{L_p} \text{ if } h_{L_p} \text{ exits from the vertex } V_p, \end{aligned} \tag{29}$$

and similarly for h_{L_q}.

From Eq. (28) we see that the face F_1 is oriented from the vertex V_p to V_q. Then

$$h_{L_{p_1}}^{\sigma(L_{p_1})} = h_{L_{p_1}}^{\prime\sigma(L_{p_1})} g_{V_p} \qquad h_{L_{q_1}}^{\sigma(L_{q_1})} = g_{V_{q_1}}^{-1} h_{L_{q_1}}^{\prime\sigma(L_{q_1})}. \tag{30}$$

On the contrary the face F_2 is oriented from V_q to V_p and we have

$$h_{L_{p_2}}^{\sigma(L_{p_2})} = g_{V_p}^{-1} h_{L_{p_2}}^{\prime\sigma(L_{p_2})} \qquad h_{L_{q_2}}^{\sigma(L_{q_2})} = h_{L_{q_2}}^{\prime\sigma(L_{q_2})} g_{V_q}^{-1}. \tag{31}$$

The face F_3 is oriented from the line L_{p_3} to L_{p_4} and we have

$$h_{L_{p_3}}^{\sigma(L_{p_3})} = h_{L_{p_1}}^{\prime\sigma(L_{p_1})} g_{V_p} \qquad h_{L_{p_4}}^{\sigma(L_{p_4})} = g_{V_p}^{-1} h_{L_{p_4}}^{\prime\sigma(L_{p_4})}, \tag{32}$$

and analogously for F_4.

We now fix g_{V_q} and change the variable from h_L to $g_{V_p} = g_{V_q} h_L^{-1}$. Using Eqs. (30)–(32), the amplitude (28) becomes

$$I(h_l) = \int \prod_{L_p\in V_p} dh'_{L_p} \prod_{L_q\in V_q} dh'_{L_q} dg_{V_p} \prod \delta_{F_1}(\dots h_{L_{p_1}}^{\prime\sigma(L_{p_1})} h_{L_{q_1}}^{\prime\sigma(L_{q_1})}\dots)\delta_{F_2}(\dots h_{L_{q_2}}^{\prime\sigma(L_{q_2})} h_{L_{p_2}}^{\prime\sigma(L_{p_2})}\dots)\delta_{F_3}(\dots h_{L_{p_3}}^{\prime\sigma(L_{p_3})} h_{L_{p_4}}^{\prime\sigma(L_{p_4})}\dots)$$
$$\times\,\delta_{F_4}(\dots h_{L_{q_3}}^{\prime\sigma(L_{q_3})} h_{L_{q_4}}^{\prime\sigma(L_{q_4})}\dots)\prod_F \delta_F(\dots.). \tag{33}$$

The integral over g_{V_p} decouples and computes to one. The new amplitude corresponds to a graph with the same faces, same connectivity, but where the line L disappeared. We identify this graph as the one obtained from $\mathcal{G}$ with the two vertices V_p and V_q contracted using the tree line L. ■

We conclude this preliminary step toward proving our main result with an observation. Note that the descendents of any tree line in the 3D graph are tree lines in the 2D graph of bubbles, because different 3D vertices always project into different 2D vertices. Hence, the number of tree lines in the 2D graph must be at least be equal to the number of tree lines which descend from the 3D tree. This allows us to give an upper bound on the number of bubbles of an arbitrary graph:

$$3(|V_{\mathcal{G}}| - 1) \leq |v_{\mathcal{G}}| - |b_{\mathcal{G}}| \Rightarrow |B_{\mathcal{G}}| \leq |V_{\mathcal{G}}| + 3. \quad (34)$$

The maximal number of bubbles decreases when taking into account the loop lines, hence improving the above bound.

B. Amplitudes and power counting for type 1 manifolds

Theorem 1.—The amplitude of a connected type 1 *manifold* vacuum 3D graph $\mathcal{G}$ is

$$A_{\mathcal{G}} = (\delta^{\Lambda}(\mathbb{I}))^{|B_{\mathcal{G}}|-1}. \quad (35)$$

Proof.—The proof is a straightforward generalization of the computation in Sec. V A. Before we proceed we need to understand better the structure of a type 1 graph.

In Fig. 6 we depicted a 3D line $L = (a', b', c') \rightarrow (a, b, c)$, and its three 2D descendents $l^{b_1} = (c'_{b'}, c'_{a'}) \rightarrow (c_b, c_a)$, $l^{b_2} = (b'_{a'}, b'_{c'}) \rightarrow (b_a, b_c)$, and $l^{b_3} = (a'_{c'}, a'_{b'}) \rightarrow (a_c, a_b)$, where the upper index of l refers to the connected component to which the 2D line belongs. As the graph is type 1, the three connected components b_1, b_2, and b_3 are all different.

Also from Fig. 6, we see that b_1 and b_2 share the two descendents of the same 3D face [the 2D strands $(c'_{b'}, c_b)$ and $(b'_{c'}, b_c)$ descend from the same 3D strand $(b', c') \rightarrow (b, c)$].

We denote the face $(c'_{a'}, c_a)$ by $f^{b_1}_{(b_1,b_2)}$, where the upper index denotes again the connected component to which the face belongs, and the lower indices denote the two connected components which share the two descendents of the 3D ancestor of the face. The same goes for the other couples of bubbles, b_1, b_3 and b_2, b_3. The situation and notations are then summarized in Fig. 20.

We now proceed to the computation of the amplitude of a type 1 graph.

Step 1.—Contraction of a tree in a connected component b'.

Consider a connected component b' in $\bar{\mathcal{G}}$. Denote $v^{b'}$, $l^{b'}$, and $f^{b'}$ the sets of vertices, lines, and faces of b'. b' is a planar connected 2D graph. As $\mathcal{G}$ is type 1, all the 2D vertices $v^{b'}$ are descendents of different 3D vertices $V^{b'}$ of $\mathcal{G}$ and all 2D lines $l^{b'}$ are descendants of different 3D lines $L^{b'}$.

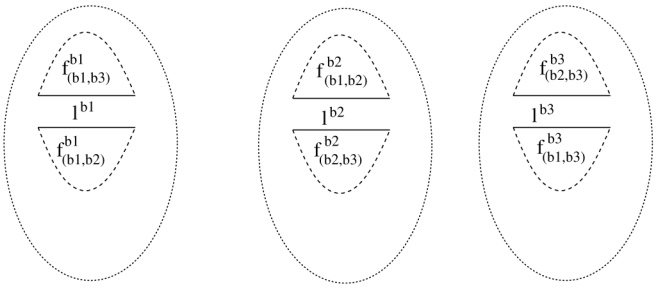

FIG. 20. The three 2D descendents of the same 3D ancestor.

Chose $\mathfrak{t}^{b'}$ a set of $|v^{b'}| - 1$ lines forming a tree in the connected component b'. We denote by $\mathcal{T}^{b'}$ the 3D ancestor of this set in $\mathcal{G}$. We prove now that $\mathcal{T}^{b'}$ does not form any loops in the graph $\mathcal{G}$, i.e., it is itself a 3D tree; in general, it would not be a maximal tree though, but simply a set of tree lines; this can be easily checked by looking at specific examples. This fact is not trivial and in fact depends on the type 1 condition for $\mathcal{G}$. So it is at this point that the assumption that our graph is type 1 plays a crucial role.

The proof goes as follows. Suppose $\mathcal{T}^{b'}$ has a loop in $\mathcal{G}$. Consider $V_1, \ldots V_k$ and $L_1, \ldots L_k$ the 3D vertices and lines belonging to this loop. V_1 is connected by L_1 with V_2, which is connected by L_2 to V_3, and so on until we reach V_k which is connected by L_k with V_1. Because $\mathcal{G}$ is type 1, L_1 has a unique descendent on b', called l_1, and V_1 and V_2 have unique descendents on b', called v_1 and v_2. l_1 necessarily connects v_1 and v_2. Iterating we find that $l_1, \ldots, l_k$ forms a loop in b', which contradicts the hypothesis that $\mathfrak{t}^{b'}$ is a tree.[8]

Therefore, $\mathcal{T}^{b'}$ is a set of 3D tree lines, as anticipated. We now proceed by contracting all 3D lines in this set using the procedure described in Sec. VI A. By lemma VI.1 the amplitudes are invariant under the contraction. The result from the 2D perspective is to contract *all* the 2D descendents of the tree lines in $\mathcal{T}^{b'}$.

Thus the 2D graph b' reduces to a planar rosette, called b. We now focus on this 2D structure.

Step 2.—Deletion of the lines of b.

Consider a line l^b on the boundary of the bubble b. It bounds two faces $f^b_{(b,b_1)}$ and $f^b_{(b,b_2)}$. The 3D ancestor L^b of l^b has another two descendents. The first is $l^{b_1} \in b_1$

[8]If, on the contrary a vertex, let us say V_2, had 2 descendents on b', then l_1 and l_2 could connect each to a different descendent. Then the loop in $\mathcal{G}$ does not need to project into a loop in b'. This is why we need the first condition in the definition of type 1 graphs.

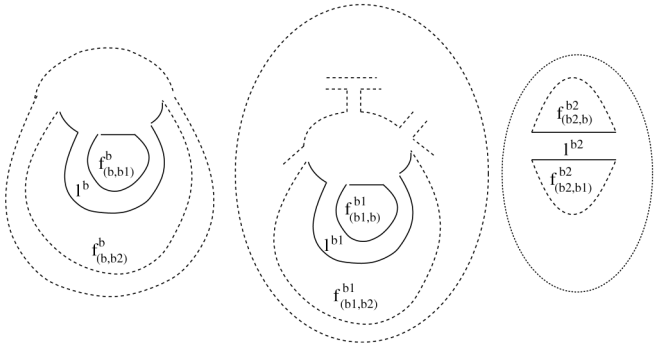

FIG. 21. The first case.

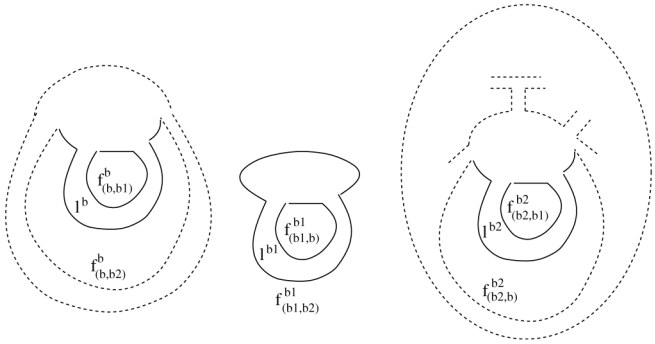

FIG. 22. The second case.

bounding $f^{b_1}_{(b_1,b)}$ and $f^{b_1}_{(b_1,b_2)}$ and the second is $l^{b_2} \in b_2$ bounding $f^{b_2}_{(b_2,b)}$ and $f^{b_2}_{(b_2,b_1)}$.

As the component b is nonempty, there exist at least one face of b bounded by only one line. Such a face exists, as the rosette b is planar, thus having only lines which do not cross. We call such a face ''simple.''

Let $f^b_{(b,b_1)}$ be a simple face, bounded only by the line l^b. Then $f^{b_1}_{(b_1,b)}$ is also simple as the two faces share the same 3D ancestor. We necessarily fall in one of the following four cases:

(i) $f^b_{(b,b_2)}$ is not simple and $f^{b_1}_{(b_1,b_2)}$ is also not simple.

(ii) $f^b_{(b,b_2)}$ is not simple, but $f^{b_1}_{(b_1,b_2)}$ is simple.

(iii) $f^b_{(b,b_2)}$ is simple, but $f^{b_1}_{(b_1,b_2)}$ is not simple.

(iv) Both $f^b_{(b,b_2)}$ and $f^{b_1}_{(b_1,b_2)}$ are simple.

Case 1 is depicted in Fig. 21.

The integral corresponding to h_{L^b} is

$$\int dh_{L^b}\delta(h_{L^b})\delta(h_{L^b}f)\delta(h_{L^b}g) = \delta(f)\delta(g), \qquad (36)$$

where f and g are nontrivial group elements associated to the 3D ancestors of the two faces $f^b_{(b,b_2)}$ and $f^{b_1}_{(b_1,b_2)}$.

The graph $\mathcal{G}$ has the property P, namely $\bar{\mathcal{G}}^{b_1} \cap b_i$ is such that no two faces share a line. Then, if the internal face of some connected component is not simple, the connected component has at least two vertices.[9] This implies that l^{b_2} is necessarily a *tree* line on the bubble b_2, as the face $f^{b_2}_{(b_2,b)}$ is not simple.

The consequence of this integration is that the lines l^b and l^{b_1} are deleted and the line l^{b_2} is *contracted*, as it is a tree line in b_2 (see Fig. 21). As long as we remain in this case we proceed by iterating Step 2.

Case 2 is depicted in Fig. 22.

[9]As any two vertices belonging to this face can be contracted *only* by propagators belonging to the face.

This is actually excluded for a type 1 graph as $b_1 \setminus \bar{\mathcal{G}}^b$ contains at least a line and thus $f^{b_1}_{(b_1,b)}$ and $f^{b_1}_{(b_1,b_2)}$ cannot both be simple at the same time.

Case 3 is depicted in Fig. 23.

The integral corresponding to h_{L^b} is

$$\int dh_{L^b}\delta(h_{L^b})\delta(h_{L^b}g) = \delta(\mathbb{I})\delta(g), \qquad (37)$$

where g is the nontrivial group elements associated to the 3D ancestor of the faces $f^{b_1}_{(b_1,b_2)}$. In this case the lines l^b, l^{b_1}, and l^{b_2} are all loop lines in the bubbles b, b_1, and b_2.

The consequence of the integration is that they are all deleted. Moreover, the bubble b disconnects: it has no remaining lines (see Fig. 23). This leads to a global factor $\delta(\mathbb{I})$ in the amplitude.

Iteration.—The contraction of a tree in b_1 shrinks its 3D ancestor $\mathcal{G}^{b_1}$ to a graph having a unique 3D vertex (of arbitrary coordination), call it V_b, and some 3D tadpole lines (that is 3D lines which start and end on the vertex V_b). The subsequent deletion of all loop lines of b_1 further simplifies this graph (that is, it eliminates the tadpole lines which have some descendant belonging to b).

As the graph is type 1, $b_2 \cap \bar{\mathcal{G}}^{b_1}$ is connected. Consequently the factoring out of b_1 contracts this connected subgraph graph to a 2D vertex, say v_b. Thus the 3D vertex V_b projects on the bubble b_2 into a *unique* vertex v_b. This

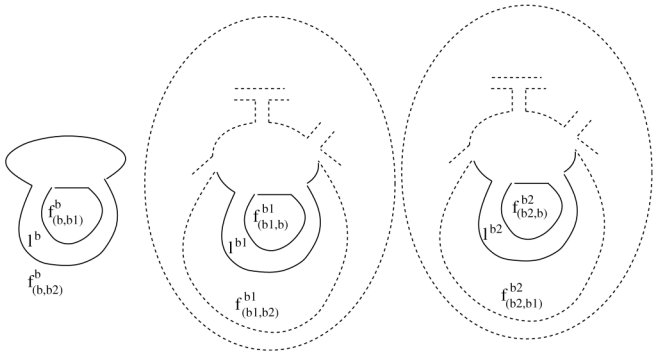

FIG. 23. The third case.

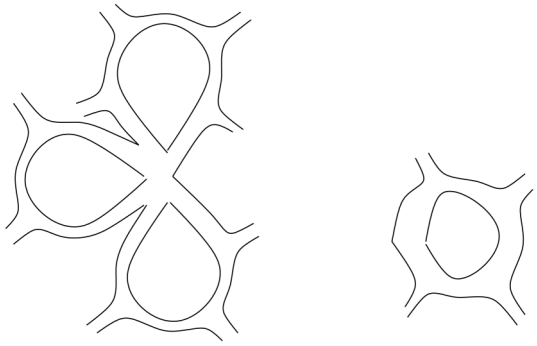

FIG. 24. $\bar{\mathcal{G}}^{b_1} \cap b_j$ after the contraction of b_1.

allows us to iterate the step 1, as the ancestor of a 2D tree on b_2, is a set of 3D tree lines.

Moreover, after factoring out the fist bubble b_1, all the subgraphs $\bar{\mathcal{G}}^{b_1} \cap b_k$ are fully contracted to points. Because of lemma III.1, we see that $\bar{\mathcal{G}}^{b_2} \cap b_j$ is a set of faces such that no two of them share a line (then typically a situation like in Fig. 24).

Hence the property P is preserved, and we can iterate.

Case 4 is depicted in Fig. 25.

The integral corresponding to h_{L^b} is

$$\int dh_{L^b} \delta(h_{L^b}) \delta(h_{L^b}) \delta(h_{L^b}) = \delta(\mathbb{I})^2. \tag{38}$$

Note that at this point we have exhausted all the lines in a 3D connected component. For every bubble we factored out either by case 2 or by case 3 we obtained a $\delta(\mathbb{I})$ factor. For the last three bubbles (case 4) we obtained only a $(\delta(\mathbb{I}))^2$ factor. We conclude that the amplitude of a type 1 manifold graph is

$$A_{\mathcal{G}} = (\delta^{\Lambda}(\mathbb{I}))^{|B_{\mathcal{G}}|-1}. \tag{39}$$

■

We have thus established the complete power counting of divergences for the type 1 graphs. Notice that in general, one expects [17,30] the amplitude for the Boulatov model to be given by some divergent factor (in absence of regularization) times a function of the combinatorial structure of the graph and on the specific group chosen [here $SU(2)$] which is a topological invariant of the (pseudo)manifold it corresponds to. Our result seems to suggest that type 1 graphs are those for which this invariant evaluates to one.

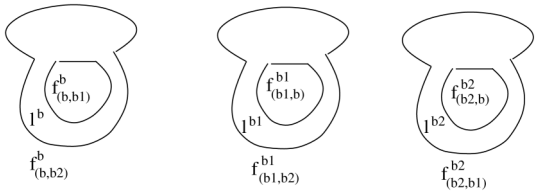

FIG. 25. The fourth case.

For example, in the Turaev-Viro regularization, based on $SU(2)_q$ with q a root of unity, this invariant would be one if and only if the graphs provide a cellular decomposition of a three-sphere; if this would hold in our setting as well, it would imply that type 1 graphs correspond to manifolds of trivial topology (i.e., spheres), thus lending further support to our second conjecture that they should dominate in some appropriate scaling limit, as this is exactly what happens in the similar matrix models. However, the relation between the (divergent) Boulatov/Ponzano-Regge model and the Turaev-Viro model is nontrivial, and such a conclusion cannot be drawn so easily in our case.

VII. CONCLUSIONS

In this paper, we have made the first steps in a systematic study of GFT renormalization, focusing on the simple and well-known Boulatov model for 3D quantum gravity. We have thus developed tools that should be later applied to other models, and identified some of the difficulties involved in applying renormalization ideas to GFTs. This 3D model, in fact, has proven to be highly nontrivial, from the point of view of renormalization, due to the complicated combinatorial and topological structure of its Feynman diagrams, given by 3D cellular complexes. Of course, this makes it also a very interesting special type of quantum field theory.

The divergences of this model come from bubbles, i.e., from the 3D cells of the Feynman diagrams, dual to vertices of the corresponding 3D simplicial complexes. As a first result, we have defined a precise algorithm for constructing the 2D triangulations that characterize the boundary of the 3D bubbles of an arbitrary 3D GFT Feynman diagram.

Introducing an explicit cutoff in the spectrum of the propagator, we have then shown that the only family of graph for which a full contraction procedure exists, and that can thus be considered local from the point of view of renormalization, are the type 1 manifolds defined in Sec. III. This means that, in order to be able to renormalize this model, we should be able to find a regime in which all divergent diagrams are type 1.

For these type 1 diagrams, we have finally proven a power counting theorem. As it is the case with matrix models, this power counting is not uniform in the number of internal vertices. We then conjecture that the regime in which these diagrams are the dominant ones, and where a proper GFT renormalization can be defined, is to be obtained by means of an appropriate scaling limit. We have also exhibited a counterexample showing that this result can not be extended to arbitrary (pseudo)manifolds.

These first steps in understanding GFT renormalization serve to clarify several key aspects of the physics of GFT models and of nonperturbative quantum gravity in general. Most importantly, as discussed in the Introduction, they

shed light on the emergence of the continuum and manifoldlike structure of quantum spacetime.

ACKNOWLEDGMENTS

We thank J. Magnen, V. Rivasseau, and M. Smerlak for discussions. D. O. gratefully acknowledges financial support from the Alexander Von Humboldt Foundation. Research at the Perimeter Institute is supported by the Government of Canada through Industry Canada and by the Province of Ontario through the Ministry of Research and Innovation.

[1] *Approaches to Quantum Gravity: Toward a New Understanding of Space, Time and Matter*, edited by D. Oriti (Cambridge University Press, Cambridge, 2009).
[2] D. Oriti, Rep. Prog. Phys. **64**, 1703 (2001); A. Perez, Classical Quantum Gravity **20**, R43 (2003).
[3] C. Rovelli, *Quantum Gravity* (Cambridge University Press, Cambridge, 2006).
[4] R. Williams, in Ref. [1].
[5] J. Ambjorn, J. Jurkiewicz, and R. Loll, Phys. Rev. D **72**, 064014 (2005); Contemp. Phys. **47**, 103 (2006).
[6] L. Freidel, Int. J. Theor. Phys. **44**, 1769 (2005).
[7] D. Oriti, in Ref. [1].
[8] D. Oriti, in *Quantum Gravity*, edited by B. Fauser, J. Tolksdorf, and E. Zeidler (Birkhaeuser, Basel, 2007).
[9] F. David, Nucl. Phys. **B257**, 45 (1985); P. Ginsparg, arXiv: hep-th/9112013.
[10] M. Gross, Nucl. Phys. B, Proc. Suppl. **25**, 144 (1992).
[11] J. Ambjorn, B. Durhuus, and T. Jonsson, Mod. Phys. Lett. A **6**, 1133 (1991).
[12] N. Sasakura, Mod. Phys. Lett. A **6**, 2613 (1991).
[13] S. B. Giddings and A. Strominger, Nucl. Phys. **B321**, 481 (1989); S. Coleman, Nucl. Phys. **B310**, 643 (1988); M. McGuigan, Phys. Rev. D **38**, 3031 (1988); T. Banks, Nucl. Phys. **B309**, 493 (1988).
[14] M. Reisenberger and C. Rovelli, Classical Quantum Gravity **18**, 121 (2001).
[15] D. Oriti, arXiv:0710.3276.
[16] R. De Pietri and C. Petronio, J. Math. Phys. (N.Y.) **41**, 6671 (2000).
[17] D. Boulatov, Mod. Phys. Lett. A **7**, 1629 (1992).
[18] M. Disertori, R. Gurau, J. Magnen, and V. Rivasseau, Phys. Lett. B **649**, 95 (2007).
[19] J. Engle, R. Pereira, and C. Rovelli, Phys. Rev. Lett. **99**, 161301 (2007); Nucl. Phys. **B798**, 251 (2008).
[20] L. Freidel and K. Krasnov, Classical Quantum Gravity **25**, 125018 (2008).
[21] E. R. Livine and S. Speziale, Phys. Rev. D **76**, 084028 (2007).
[22] D. Oriti, arXiv:0902.3903.
[23] V. G. Turaev and O. Y. Viro, Topology **31**, 865 (1992).
[24] R. Gurau, J. Magnen, V. Rivasseau, and F. Vignes-Tourneret, Commun. Math. Phys. **267**, 515 (2006).
[25] L. Freidel and D. Louapre, Classical Quantum Gravity **21**, 5685 (2004).
[26] R. De Pietri, L. Freidel, K. Krasnov, and C. Rovelli, Nucl. Phys. **B574**, 785 (2000).
[27] L. Freidel and D. Louapre, Nucl. Phys. **B662**, 279 (2003).
[28] L. Freidel and D. Louapre, arXiv:gr-qc/0410141.
[29] J. Barrett and I. Nash-Guzman, Classical Quantum Gravity **26**, 155014 (2009).
[30] H. Ooguri, Prog. Theor. Phys. **89**, 1 (1993).